

Chapter 2.3

Active Cell Processes: Motility, Muscle, and Mechanotransduction

2.3.1 Introduction

In this chapter, we address the active processes relating to cell mechanics, where the biology and mechanics become inseparable. In contrast to the previous two chapters, this one will be more qualitative, and the models, to the extent they exist, more ad hoc. This is because not only are the processes much more complex, often involving a cascade of reactions or numerous individual cell functions, but they are also less well understood.

We begin this chapter with a discussion of the various types of active cell processes involving motility in some form. These range from the motion of cilia and flagella, to phagocytosis, to cell migration along a substrate. Other phenomena on a smaller scale provide the energy for these motions, as discussed more fully in Section 1. Models for cell motility will be described next, and then the methods that have been developed to quantify it. We also include in this chapter a description of muscle and active cell contraction, beginning with a macroscopic perspective, but extending down to the level of individual cross-bridge dynamics and the models that are used to describe it. This chapter ends with a discussion of mechanotransduction. Contrary to most of the literature on this topic, however, the focus here is on the mechanisms by which force is transduced into a chemical signal, rather than on the subsequent signaling cascade that leads to the ultimate response of the cell. Because these are poorly understood, and the hypotheses still require validation, this section should be viewed as a basis for further study, and not a definitive description of known phenomena. This remains one of the most challenging, and fascinating, areas of biomechanics research.

2.3.2 Cilia and Flagella

Molecular structure. Cilia and flagella are essentially the same in terms of their internal structure and the molecular mechanism by which they produce movement. The primary difference is that a cell typically has only one or several flagella, whereas ciliated cells (Fig. 2.3.1) have many cilia often as high as $10^9/\text{cm}^2$.

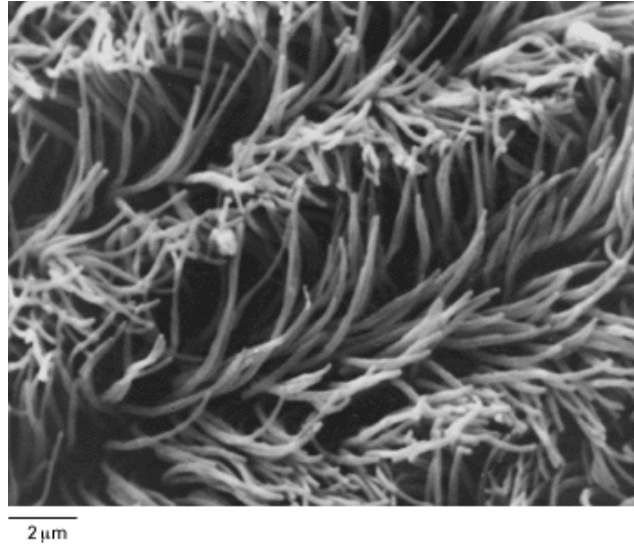


Fig. 2.3.1. A view looking down onto a collection of ciliated cells. (Reproduced from (Alberts, Johnson et al. 2002))

Their function differs as well. Whereas flagella are generally used for motility (e.g., sperm, certain types of bacteria), cilia are most commonly found on fixed cells and are used to generate a flow of liquid past the cell. One example is in the pulmonary airways where cilia are used to propel the layer of liquid that lines the airways of the lung, containing mucus, particulate matter, and cell debris, toward the mouth for the purpose of clearance.

Because they serve different purposes, they also exhibit different patterns of movement. Cilia need to produce rectified motion of the surrounding fluid, in a direction parallel to the surface of the cell. Their motion therefore, consists of a forward stroke in which they maximize the force they exert by viscous drag on the external fluid by making themselves relatively straight, followed by a reverse stroke in which they double up, and orient themselves nearly tangent to their direction of motion, to reduce drag [Fig. 2.3.2(a)]. Cilia beat nearly in synchrony, giving rise to a wavelike appearance, much like the gentle undulations in a field of wheat caused by the wind. Flagella, by comparison, are more symmetric in their motion since their object is to propel the cell forward, in a direction essentially parallel to the mean axis of the flagellum [Fig.

2.3.2(b)]. Their movement appears as a sinuous wave that propagates from the body of the cell toward the tip of the cilium. The dimensions of a single filament can range from a few microns up to nearly 2 mm for some flagella. Their diameter, however, is quite uniform at about $0.25\mu\text{m}$.

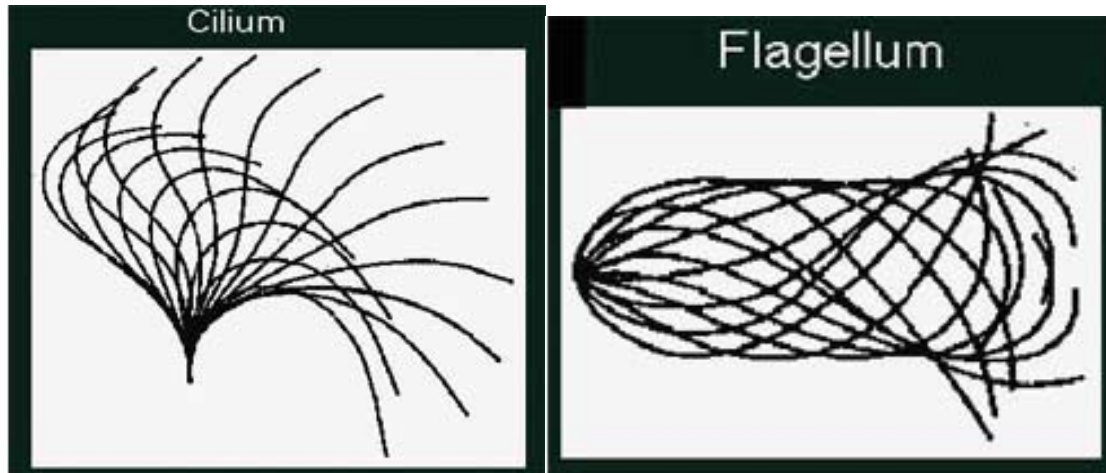


Fig. 2.3.2. Sketches showing the trajectory of a single cilium (left) and flagellum (right). Motion of the cilium is such that the rightward movement occurs when the filament is stretched out straight, and the leftward movement occurs when the filament is bent, tending to drive the surrounding fluid from left to right. Motion of the flagellum is more symmetric as successive waves appear at the point of attachment to the cell (on the left) and propagate toward the tail on the right, producing a forward propulsive force on the cell.

All cilia and the flagella in eukaryotic cells share a common structure and move by means of bending produced in a distributed manner along their entire length with their base rigidly fixed at the cell body. The key to their motion is in the axoneme, a unique arrangement of microtubules and cross-linking proteins (Fig. 2.3.3). Commonly referred to as the “9 + 2” arrangement, the microtubules form an outer circumference consisting of nine pairs. In each pair, one of the microtubules is incomplete forming a “CO” type of doublet. In the center is located a pair of single microtubules. Bending deflections are produced by the outer doublets that are connected by fixed cross-links (nexin) that prevent sliding, in combination with moveable ciliary dynein. Dynein is a motor protein that hydrolyzes ATP to move toward the negative end of a microtubule -- away from the cell body in this instance. As the dynein motors attempt to produce a sliding motion between adjacent microtubules in the outer ring, the stiffness provided by the nexin converts the sliding motion into a bending deformation. By appropriate coordination, communicated via the radial spokes (Fig. 2.3.3), the complex patterns of bending seen in the movements of cilia and flagella (Fig. 2.3.2) can be readily produced.

We should note that, by contrast, flagella in many bacteria have a different structure and move by an entirely different mechanism, with the flagellum being driven by a molecular motor located at its base, powered by a flow of protons. These motors rotate at speeds as high as 100 revolutions per second, propelling the bacterium in a series of “runs” where it can move at speeds of $20 \mu\text{m/s}$ for a period of about 1 second, interspersed with periods of “tumbling”, each lasting about 0.1 s during which the flagellar movements are uncoordinated. An important structural characteristic of bacterial flagella is their high stiffness, which is evident from their persistence length, which is on the order of 1 mm.

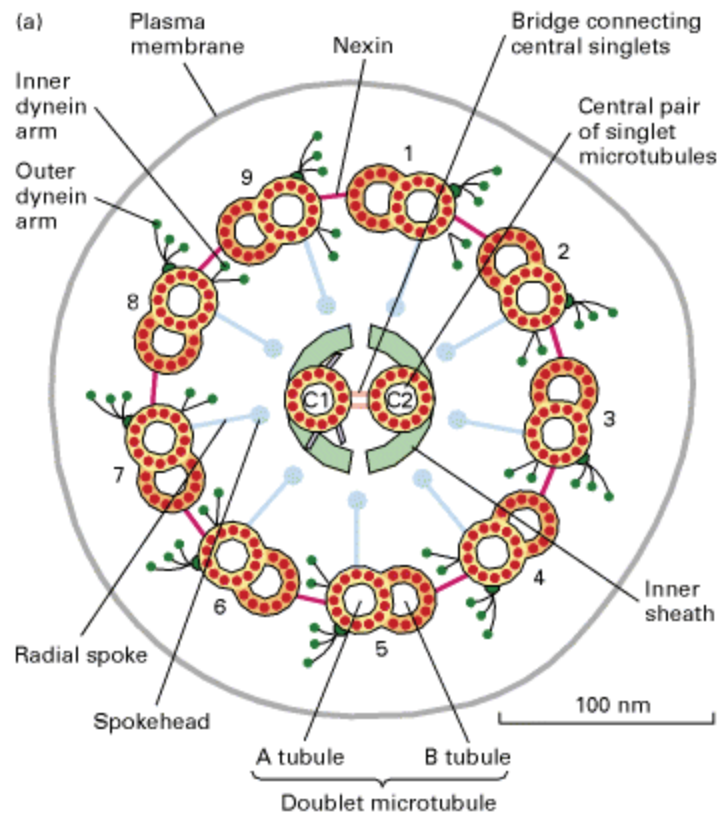


Fig. 2.3.3. Cross-sectional sketch showing the internal structure of a flagellum or cilium. Note the “9+2” arrangement with 9 pairs of microtubules (doublets) around the outer circumference and one pair of single microtubules in the center. Neighboring doublets are firmly attached with nexin cross-links and also tethered to dynein, a motor protein (reproduced from (Lodish, Berk et al. 2000)).

*Mechanism of thrust generation in flagella*¹. As the bending wave propagates along the flagellum, the viscous interaction forces with the surrounding fluid give rise to a net forward

¹ The author is indebted to Prof. T.J. Pedley for his contributions to this section.

thrust on the body (Lighthill 1969). Here we consider the bending deflection to be a wave of unchanging form as it propagates from the body of the cell in the rearward direction (Fig. 2.3.4). We take V to be the speed of the wave in the z -direction and c its speed along s relative to the centerline of the filament, so that $V = \alpha c$ where α is the ratio of the wavelength along z to the wavelength along s . The speed of the cell is $-U$. Therefore, to an observer traveling with a point of fixed wave amplitude on the wave (at speed $V-U$ relative to the stationary fluid far from the cell), the speed at which a material point is observed moving forward tangent to the filament along s , is c . Thus, the net velocity of a material point relative to a fixed reference frame is

$$-w = (V - U)i - ct \quad (1)$$

where i is a unit vector in the z -direction and t is the unit tangent vector. To an observer sitting on a material point, the fluid appears to be approaching at the velocity w , which can be decomposed into components in the normal and tangential directions:

$$w_n = w \cdot n = (U - V)(i \cdot n) \quad \text{and} \quad w_t = w \cdot t = (U - V)(i \cdot t) + c \quad (2)$$

The normal and tangential components of force (per unit length of filament) can be expressed as

$$f_n = K_n w_n \quad \text{and} \quad f_t = K_t w_t \quad (3)$$

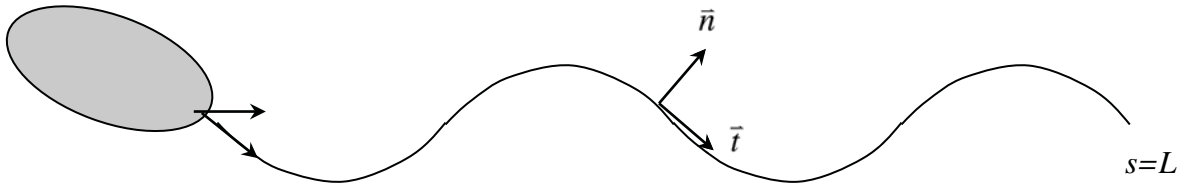


Fig. 2.3.4.

where K_n and K_t are the viscous drag coefficients for normal and tangential flow, respectively, past the local segment of filament, and $K_n/K_t \approx 2$. Finally, to obtain the net force acting on the filament segment in the direction of motion (the propulsion force, F_p) one needs to obtain the force component in the negative z direction taking the scalar product of f and i , and integrating along the length of the filament:

$$-F_p = F_z = \int_0^L (f_n n \cdot i + f_t t \cdot i) ds \quad (4)$$

Combining Eqns. (1) to (3) and recognizing that $w \cdot i = (w \cdot n)(n \cdot i) + (w \cdot t)(t \cdot i)$, one obtains:

$$-F_p = (K_t - K_n) \int_0^L (w \cdot t)(t \cdot i) ds + K_n \int_0^L (w \cdot i) ds \quad (5)$$

and, with further substitution from above:

$$-F_p = (K_t - K_n)(U - V) \int_0^L (t \cdot i)^2 ds + K_n(U - V)L + K_t c \int_0^L (t \cdot i) ds \quad (6)$$

which can be simplified to obtain:

$$F_p = (V - U)[(K_t - K_n)\beta L + K_n L] - K_t VL \quad (7)$$

where $\beta L \equiv \int_0^L (t \cdot i)^2 ds$ and $\alpha L \equiv \int_0^L (t \cdot i) ds = VL/c$. If we express this in dimensionless form, we can write:

$$\frac{F_p}{VK_n L} = \left(1 - \frac{U}{V}\right) [(\gamma - 1) + 1] - \gamma \quad (8)$$

The speed of motion of the cell or organism will be determined by a balance between this force of propulsion and the drag of the surrounding fluid on the cell. If we take the latter to have a form similar to that for the flagellum, we can therefore express it as $UK_n L \delta$ where δ is a constant of order unity and K_n is the drag coefficient used in the equations above. One can then solve for the dimensionless cell velocity:

$$\frac{U}{V} = \frac{(1 - \beta)(1 - \gamma)}{1 + \delta - \beta(1 - \gamma)} \quad (9)$$

In evaluating this expression, choosing the correct value of γ is troublesome, but it has been shown that a value of 0.5 gives reasonable agreement with many experiments [ref]. Also, although δ depends on the shape and size of the cell, if we choose $\delta = 1$, and set $\beta = 0.5$, the ratio of cell speed to wave speed is 0.14.

2.3.3 Budding of vesicles – phagocytosis, exocytosis and endocytosis

[in progress]

2.3.4 Cell migration through tissues and on surfaces

Why do cells migrate?

In Chapter 2.1, the process by which leukocytes adhere to the wall of a blood vessel was described, involving first transient adhesion and rolling, and eventually firm attachment to the wall, mediated by various adhesive receptor-ligand interactions. Having adhered to the endothelium, the cell then migrates to an intercellular junction and squeezes through a narrow gap typically no more than $0.1 \mu\text{m}$ wide. Once on the other side, it continues to migrate through the extracellular matrix of the tissue in the direction of infection, lured by a gradient in chemotactic agents. Other cells may have different reasons for migration. Migration is an essential element in growth and development, but also plays a critical role in the metastatic spread of cancer cells. Fibroblasts, normally sedentary factories of extracellular matrix components, become motile when the need arises to repair damaged tissue. Epithelial or endothelial cells can also be induced to migrate in order to provide a continuous protective coating over newly exposed tissues. In this case, as with several other cell types, cell migration can be initiated by the absence or loss of cell-cell contact, and terminated by the formation of new junctions.

While cell migration is essential for life, it also has a detrimental side. Cancerous cells migrate from the primary tumor, enter the circulation, and eventually adhere to the vessel wall and migrate out into the surrounding tissue and initiate a metastatic tumor. Many recent experimental treatments for cancer are directed at inhibiting the ability of tumor cells to migrate.

Experimental measurement of cell migration

In a typical experiment, the migration pattern and speed of a cell over a two-dimensional substrate can be traced microscopically and mapped out as in Fig. 2.3.5. Unless a chemotactic signal is present, the path of the cell as viewed over long times is random and can be described in terms of a diffusivity, analogous to the thermal motion of individual molecules in a gas. Over short times, the cell's motion can be described as a sequence of short-duration movements in specific directions interspersed with periods of random reorientation. When viewed over a sufficiently long time, the cell therefore appears to move randomly, losing track of the direction in which it was previously headed. This type of migratory pattern has been termed a *persistent random walk* and can be characterized by two independent parameters, a persistence time t_p and a cell speed V_c . The diffusivity of the cell motion D can be shown, on purely dimensional grounds, to be proportional to $V_c^2 t_p$. It may also be useful to think in terms of a persistence

distance, the product of persistence length and speed, as this is clearly analogous to the persistence length of a protein or strand of DNA as discussed in Section 1.

Different cell types migrate with different speeds. Among human cells, speeds can range from as high as $20 \mu\text{m}/\text{min}$ for neutrophils, to as low as $0.2 \mu\text{m}/\text{min}$ for melanoma cells (Fig. 2.3.6). This range can be compared to other forms of cellular motion such as the swimming of sperm ($\sim 50 \mu\text{m}/\text{min}$) or bacteria ($\sim 500 \mu\text{m}/\text{min}$), the movement of listeria (several hundred $\mu\text{m}/\text{s}$) or muscle contraction ($> 10,000 \mu\text{m}/\text{s}$).

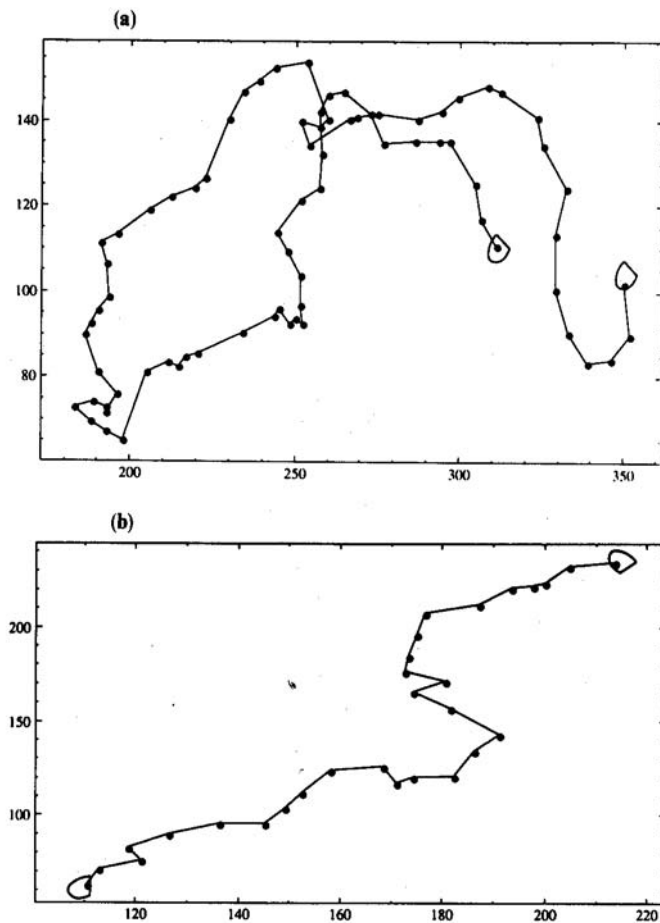


Fig. 2.3.5. Sample migration paths taken from the trajectories of two cells migrating on a 2-dimensional surface. Cell position at one minute intervals are shown by the symbols. [Reproduced with permission from (Lauffenburger and Linderman 1996).]

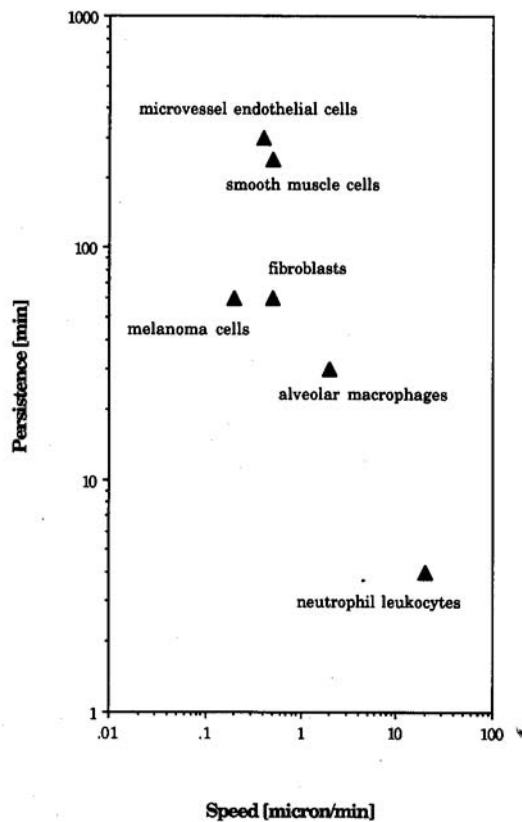


Fig. 2.3.6. Measured migration speed and persistence time for a variety of different cell types. [Reproduced with permission from (Lauffenburger and Linderman 1996).]

One method that has been employed to monitor the forces exerted by a single cell during migration is by the use of a highly flexible substrate, produced by cross-linking the surface of a silicone fluid pool. When cells contract, the substrate then buckles, forming what have been termed “Harris wrinkles” (Harris 1984). While this has been useful as a qualitative demonstration of cellular contractile forces, it has been difficult to obtain much quantitative information from these experiments. Contact stresses can be quantified if the cells are plated onto a compliant gel into which has been seeded small microspheres as markers. By monitoring the displacement of each bead as a cell passes, the stress distribution that the cell exerts on the substrate can be inferred. In this way, average contact stresses have been found to fall in the range of 2000 N/m^2 with peak values as high as $10,000 \text{ N/m}^2$ for a migrating 3T3 fibroblast (Dembo and Wang 1999).

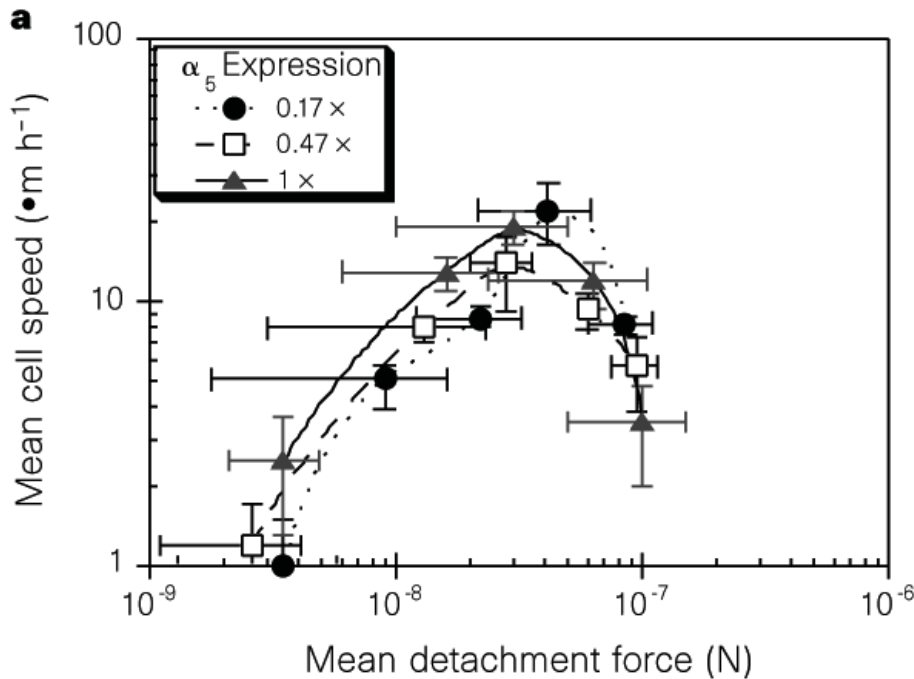


Fig. 2.3.7. As the force required to detach a cell from its substrate (a measure of the strength of adhesion) increases, the cell migration speed first increases, reaches a maximum, and then falls steeply. At low levels of detachment force, the cells will tend to be more rounded whereas the strongly adherent ones will be in a flattened state. [Reproduced from (Palecek, Loftus et al. 1997)]

A model for cell migration

Just as there exist a variety of different types of molecular motor, cells, too, exhibit a variety of modes of locomotion. Some differ in obvious ways – e.g., a swimming sperm contrasted against a migrating neutrophil -- but even among the different migrating cells significant differences exist. Rather than attempt to describe all the various theories and modes of migration, we focus here on just one, for which reasonably strong empirical support exists.

Any model for cell migration must incorporate the following general features:

- *Directionality.* Even cells that migrate randomly exhibit periods during which it has a definite directional preference. In cells sensing a gradient in some chemoattractant, this preference is particularly strong, leading to a net directed movement over extended periods of time. In order to accomplish this feat, the cell must become asymmetric or polarized in the sense that the front end undergoes processes that differ from those occurring near the back end.

- *Force transmission to the cell's surroundings.* In order to propel itself, the cell must have some means of exerting a force on the surrounding medium, be it fluid or solid. For the bacteria discussed in Section 2.3.2, the interaction was mediated by the viscous drag between the flagellum and the surrounding fluid. In the case of migration on a 2-dimensional surface, these forces are typically transmitted via the adhesion receptors embedded within the cell membrane, and as we have just seen, can be remarkably high.
- *Active force generation.* As with nearly every directed motion, forces must be generated and energy is consumed. The origin of the force may occur at the molecular scale (e.g., the molecular motors discussed in Section 1), and may involve stochastic processes (e.g., the Brownian ratchet). Models need to provide a mechanism and identify the fuel for energy production.

The following model incorporates each of these features, and is used to describe the directed motion of a cell adhering to a 2-dimensional substrate. Many of the same elements may be applicable in 3-dimensional migration through a matrix, but we understand that process much less well at this point in time.

[A wealth of images and movies showing the migration of various types of cell can be found on the internet. For some interesting links, try: <http://www.cellmigration.org/sciMovies.html> or http://vlib.org/Science/Cell_Biology/cytoskeleton.shtml]

Polarization. As a cell prepares for migration, it needs to become polarized, thereby identifying the direction in which it will travel. It is obvious that asymmetries must develop. These primarily take the form of a redistribution of cytoskeletal components (actin, microtubules), and adhesion receptors. The outward appearance of the cell might change as well, with gross asymmetries appearing, but these are most evident once the cell is under way.

Protrusion and Adhesion. Once polarization has occurred, the stage is set for migration. The simplest way to envision migration is that the cell physically reaches out from its leading edge, by the formation of lamellipodia (sheet-like protrusions) or filopodia (finger-like protrusions). Often associated with these structures, is a general ruffling or undulation near the leading edge of the cell. These protrusions can occur in different ways, but the “Brownian ratchet” is one mechanism for which there is strong experimental support. In this model for protrusion, the actin cytoskeleton extends by polymerization to a location right adjacent to the membrane at the

leading edge. Both the actin filaments and the membrane, however, are fluctuating due to thermal motions, so the distance between the tips of the actin filaments and the membrane varies with time. If local conditions are favorable for further growth of the filaments by polymerization, whenever the distance between the membrane and the matrix is large enough to permit the addition of another monomer to chain, the monomer will attach, effectively filling the gap and, on average, moving the location of the membrane forward. Each time another monomer is added, the membrane is "ratcheted" to a new position and the cell progressively protrudes.

Experimental evidence supports the theory that actin polymerization plays an important role in membrane protrusion. Electron microscopy of migrating cells treated with detergent to remove the membrane so that the actin matrix is easily visible has demonstrated that the actin filaments are predominantly oriented with their barbed ends pointing toward the membrane (Fig 2.3.9). Recall from Chapter 2.2, that actin filaments grow by polymerization at the barbed end.

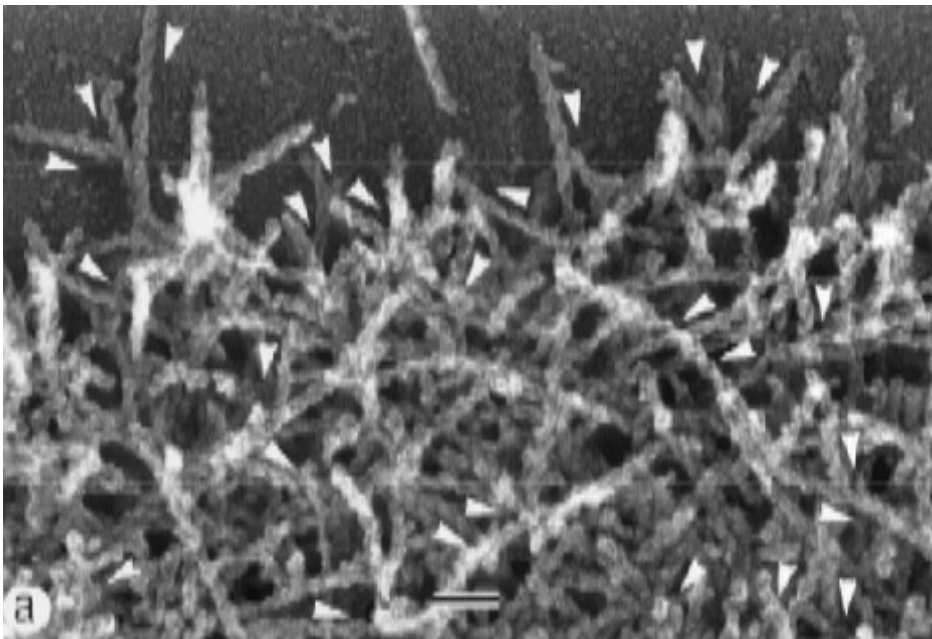


Fig. 2.3.9. An electron micrograph at the leading edge (top of figure) of a migrating keratocyte treated with detergent to visualize the cytoskeleton. Arrowheads indicate the polarity of the actin filaments, pointed or barbed. Note that nearly all the arrowheads are pointing downward, away from the leading edge, indicating that the filaments are growing upward, from the barbed end. Scale bar = 0.1 μm . [Reproduced from (Svitkina, Verkhovsky et al. 1997).]

Example: Can polymerization provide the force needed to produce membrane protrusions?
 ((Peskin, Odell et al. 1993) Howard, Ch 10).

Once the cell has formed a protrusion, by the action of a Brownian ratchet or another mechanism, it must adhere to its surroundings so that it can pull itself forward. This might occur over a two-dimensional substrate, or through a three-dimensional matrix, where the details of attachment might differ, but the result is the same. Adhesion is typically accomplished via a variety of transmembrane receptors of the integrin family, forming what are called focal adhesion complexes. These complexes can be highly transient, forming and dissipating as the cell progresses, the process mediated by a collection of signaling proteins (e.g., Rac and Cdc42). Some, however, persist and form an anchor for actin filaments in the main body of the cell, thereby providing a means of attaching the intracellular cytoskeleton directly to the surrounding matrix.

Example on the rates of actin polymerization and comparison to cell migration speeds. (Howard)

Contraction. As the cell reaches forward and grabs hold, it must then pull its body forward in order to make progress. This action likely involves the actin-myosin II system, at least in some cell types. In Chapter 1.3, it was demonstrated how myosins can effectively walk along an actin filament. Clusters of bi-polar myosin II filaments have been identified in association with the actin matrix, and concentrated in the region between the protruding lamellipodia and the main body of the cell. In this same region, the actin matrix is observed to undergo a transition from a more or less random orientation to one in which the filaments are primarily oriented parallel to the leading edge and at higher concentration. Immediately behind this zone, the actin concentration falls off rapidly, presumably indicating depolymerization into actin monomers that can then diffuse forward to once again fuel the polymerization at leading edge.

While the precise mechanism by which actin-myosin interactions produce this contraction of the cytoskeletal matrix is not clear, it seems likely that myosin II plays a role in actin filament reorganization, and in the process, contracting the matrix, pulling the front and rear portions of the cell together. One example of how this might occur is shown in Fig. 2.3.10. The myosin molecules shown in the figure are each adherent to two filaments and move along both toward the positive or barbed end. As they do, depending on the orientation of the actin filaments, the myosin might cause the actin matrix to collapse by bringing the filaments closer together. This type of collapse can condense the actin matrix into a collection of parallel filaments and in the process, produce contraction in the direction of cell motion.

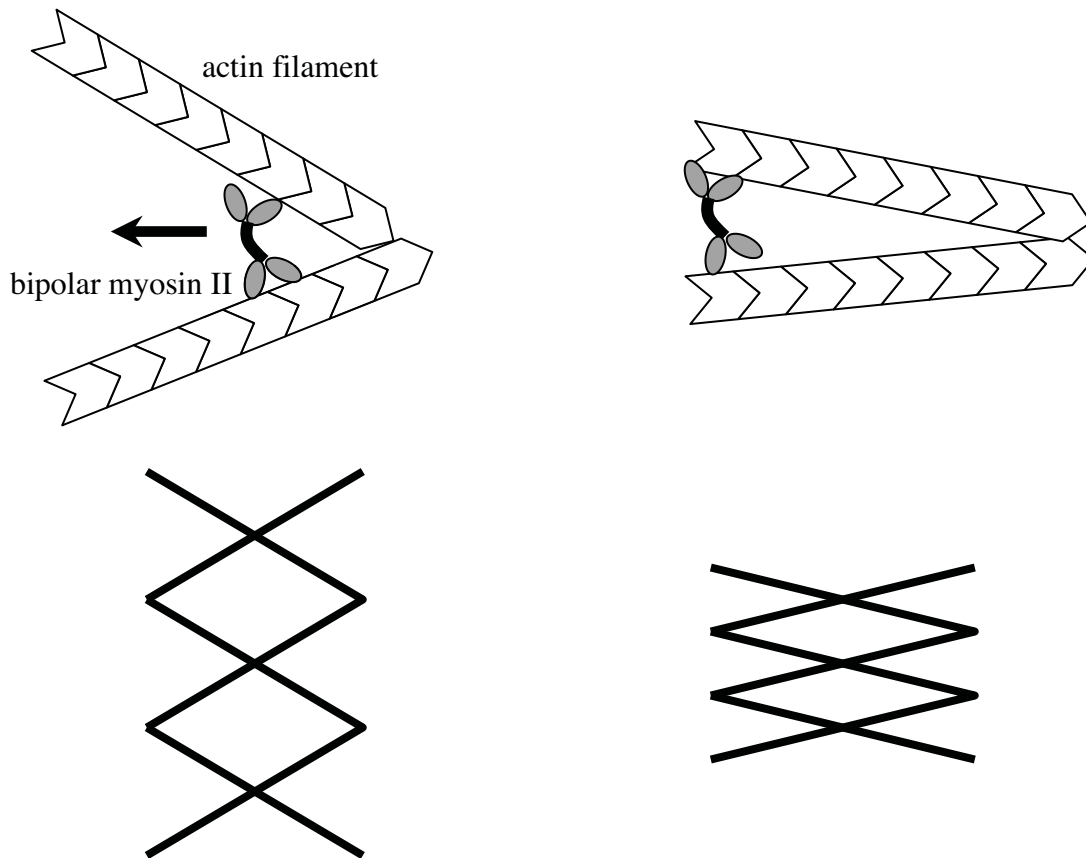


Fig. 2.3.10. One example of how the movement of bipolar myosin II along a pair of actin filaments can lead to condensation of the actin into a band of nearly parallel filaments.

Forces generated by actin-myosin mediated contraction, in non-muscle cells, of about 10^3 - 10^4 N/m² ((Felder and Elson 1990) (Kolodney and Wysolmerski 1992)) are transmitted fore and aft via the actin matrix, ultimately creating a force in the adhesion receptors. The net result of this contraction and force transmission is a rearward directed force on the external environment (e.g., the substrate or extracellular matrix) in the front part of the cell, and a forward directed force in the back, setting the stage for the next phase, rear release.

Rear release. Release of the *uropod* or trailing edge of the cell is mediated by cell polarization in that there must exist an asymmetry in the adhesion strength, either by means of a relative increase in density of adhesion complexes toward the leading edge, or an increase in the strength per bond. Either of these will lead to the situation in which the forward parts of the cell are capable of sustaining higher levels of force than the trailing regions, leading to the bonds at the trailing end giving way, allowing the cell to contract in the direction of movement.

Migration through a three-dimensional matrix. Although the process just described appears to explain much of what is seen during cell migration on a flat, two-dimensional substrate, the process of migration through a three-dimensional matrix, as is more common in vivo, may differ in some important respects. We know very little about how cells make their way through the extracellular matrix, but recent experiments (Cukierman, Pankov et al. 2001) have led to some interesting observations. The nature of cell attachment appears to be critically dependent on the three-dimensionality of the matrix, its pliability, and its composition. Adhesion complexes in 3D matrices composed of natural, extracellular matrix materials, have a different composition (favoring the $\alpha_5\beta_1$ integrin), different morphology (are more elongated and spindle-shaped), and tend to produce stronger attachments. Other adhesion-mediated activities also are affected such as migration speed and proliferation rates. While these studies of adhesion and migration in 3D matrices are just beginning, they suggest that much of what we have learned from 2D culture may not be fully applicable to the in vivo situation.

Example: Why is there an optimal level of adhesion for cell migration?

We can solidify some of these concepts by way of the following simple model for cell migration that leads to a scaling law useful in the interpretation of the effect on migration speed of cell-substrate adhesion strength. We know from discussions in Chapter 2.2, that cell shape can be altered by the strength of adhesion to a substrate. Less adherent cells tend to be more spherical and have a smaller region of contact with the substrate than more strongly adherent cells. We have also seen above (Fig. 2.3.7) that there appears to exist an optimum in adhesion strength for cell migration, in that the speed of cell migration falls if the cells become either more or less adherent than the optimum. How then, is the adhesion strength related to the speed of a migrating cell?

Consider the cell in Fig. 2.3.11, migrating on substrates with varying degrees of adhesiveness, either through variations in ligand concentration or by the use of different ligands with different affinities to the cell. For high levels of adhesion, the cell will be in a flattened configuration so that its aspect ratio, height-to-diameter, is low. For poorly adhesive conditions, the cell will become more rounded with an aspect ratio approaching unity. In both cases we consider the cell to be of constant volume with a region of adhesion of linear dimension d .

In order to proceed with the model, we need to make some assumptions. First, we assume that the cell migrates due to the work done by actin-myosin interactions inside the cell as described by the contraction phase above, and that the primary form of energy dissipation is by means of viscous shear stress inside the cell, viewed for this purpose as a viscous drop. We neglect, therefore, any differences in energy between the new bonds being formed at the leading

edge and those breaking at the trailing edge, while at the same time recognizing the need for *some* degree of asymmetry in bonding strength. Consequently, the energy loss is due to the viscous contribution which we will assume scales in the same manner as in a viscous fluid. Viscous energy dissipation per unit volume scales as the product of the fluid viscosity and the square of the velocity gradients, or:

$$\Phi \propto \mu \left(\frac{\partial v}{\partial x} \right)^2 \quad (10)$$

For the purpose of an order-of-magnitude estimate, we take the relevant velocity scale to be the cell speed, V , and arbitrarily for now define a length scale \tilde{x} over which the velocity changes occur. The rate of energy dissipation can therefore be approximated as the product of Φ , obtained by introducing these scaled variables into the expression above, and the volume within which the dissipation occurs, \tilde{V} .

The scalings for \tilde{x} and \tilde{V} depend on the particular state of the cell, whether it is in a rounded or flattened state. If rounded [Fig. 2.3.11(a)], most of the velocity gradients are confined to a region in the vicinity of the adhesion zone, so $\tilde{x} \sim a$ and $\tilde{V} \sim a^3$, leading to the following expression for the total rate of energy dissipation:

$$\int \Phi dV \propto \mu \left(\frac{V}{a} \right)^2 a^3 \quad \text{for a rounded cell.} \quad (11)$$

If sufficiently flattened [Fig. 2.3.11(b)], the velocity gradient will occur over the entire height of the cell, h , and dissipation will occur in the entire cell volume, ha^2 , leading to:

$$\int \Phi dV \propto \mu \left(\frac{V}{h} \right)^2 ha^2 \quad \text{for a flattened cell.} \quad (12)$$

An overall energy balance must exist. Therefore, based on the assumptions of the model, the rate of energy dissipation must be balanced by the rate at which work is done by the actin-myosin interactions. This can be expressed as a product of the force generated and the speed of contraction within the cell. The contraction speed is simply the cell migration speed, V . To estimate the force, recognize that in order to migrate at all, the forces must be sufficient to break the receptor-ligand bonds at the trailing edge of the cell. Consequently, the force generated within the cell must scale as the product of the adhesion force per unit area, and the area of adhesion. Combining these gives the following expression for the rate at which work is done by the molecular motors:

$$FV \propto \gamma a^2 V \quad (13)$$

which can be equated to either of the two expressions given above for the rate of energy dissipation to yield the following scaling relationships:

$$V \propto \frac{\gamma d}{\mu} \quad \text{for a rounded cell,} \quad (14)$$

and

$$V \propto \frac{\gamma h}{\mu} \propto \frac{\gamma}{\mu a^2} \cdot (ha^2) \quad \text{for a flattened cell.} \quad (15)$$

In the last of these terms, the (constant) volume of the cell has been factored out explicitly. Inspection of these expressions shows that as the area of contact to the substrate increases, as a consequence of an increase in the adhesiveness of the substrate, the speed of the cell will at first increase, pass through a maximum, then decrease.

The expression above for a nearly spherical cell can also be combined with the result from Chapter 2.1 from JKR theory (Johnson, Kendall et al. 1971). Assuming the energy of adhesion per unit area (J) can be related to the force of adhesion per unit area (γ) through a characteristic length of deformation of the adhesive "spring", denoted as δ_s , we can re-write the first expression in the form:

$$V \propto \left(\frac{\gamma^4 \delta_s R^{1/2}}{\mu^3 E} \right)^{1/3} \quad \text{for a rounded cell.} \quad (16)$$

Here again, it can be seen that an increase in adhesion force leads to an increase in migration speed for a rounded cell. Because of the assumption of small deformation in JKR theory, however, it would be inappropriate to use it for the flattened cell.

2.3.5 Muscle contraction

Linking macroscopic behavior to microscopic phenomena

Throughout this text, we have attempted to describe the mechanical properties and behavior of a biological material on the basis of its molecular composition and phenomena that occur on a molecular scale. Muscle provides an ideal opportunity to reinforce that integrative approach. Studies over the years have provided a wealth of information on muscle performance in a variety of situations, have clearly identified its structure at the molecular, cellular and tissue levels, and have elucidated the fundamental mechanisms of muscle activation and the actin-myosin interactions that produce contractile force. In this section, we summarize some of what is currently known with a focus on skeletal muscle, the other types being cardiac muscle and smooth (non-striated) muscle used to constrict arteries, airways and other organs. The reader should recognize, however, that the basic concepts are more generally applicable to these other types of muscle as well.

Observations of muscle on a macro-scale

Muscle can be thought of as having two structural elements that act in parallel: the contractile cells and the fibrous tissue that surrounds them. The cells are relatively compliant when non-activated, and the fibrous tissue therefore dominates the elastic behavior of relaxed muscle. In that situation, an intact muscle exhibits a behavior quite similar to that of other fibrous tissues in that the slope of the static stress-strain curve steepens with increasing stretch (Fig. 2.3.12, lower curve) due to progressive recruitment of an increasing number of extracellular matrix fibers. It has been observed that muscle, like many other biological materials, stiffens in such a way that the slope of the stress-strain (σ - ϵ) relation increases linearly with extension satisfying the relationship:

$$\frac{d\sigma}{d\epsilon} = \alpha(\sigma + \beta) \quad (17)$$

where α and β are empirically-based constants. Integrating, one obtains the following simple constitutive law for relaxed muscle:

$$\sigma = Ce^{\alpha\epsilon} - \beta \quad (18)$$

where C is a constant of integration.

When muscle is maximally stimulated, or *tetanized*, and the force is measured as a function of length, the contribution of the muscle cells becomes dominant. As can be seen by the difference between the upper and lower curves in Fig. 2.3.12, that *active* contribution attains a maximum when the muscle is at its resting length ($l/l_0=1$) and falls to zero when l/l_0 is approximately < 0.5 or > 1.8 . This defines the range of muscle lengths over which active contraction can generate additional force, the reason for which will become apparent when we examine the microarchitecture of a sarcomere, the fundamental unit of contraction.

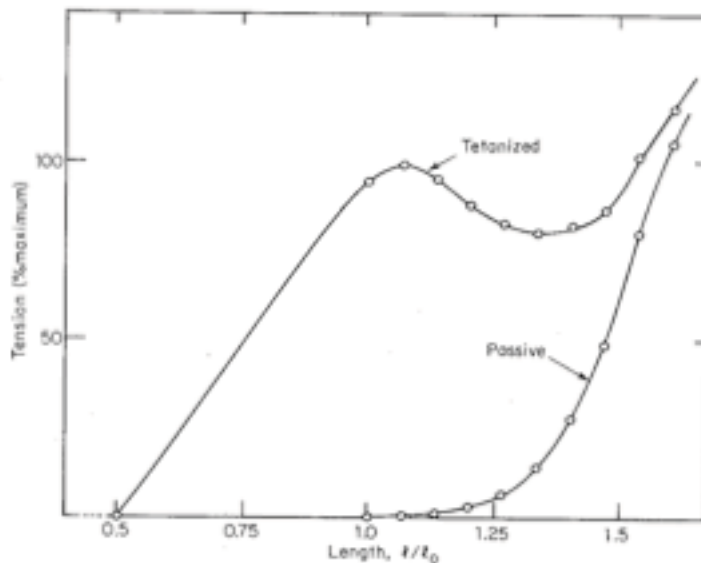


Fig. 2.3.12. The relationship between tension (normalized to maximum tension) and length (normalized to rest length) in an isolated muscle. Lower curve: relaxed. Upper curve: maximally constricted (tetanized) muscle. [Reproduced from T.A. McMahon, “Muscles, Reflexes, and Locomotion”.]

It is important to emphasize that up to now we have been discussing the static force produced by muscle at a given fixed length, under so-called *isometric* conditions. More commonly, however, muscles are used in situations in which they simultaneously generate force and are either contracting or elongating, as in the act of riding a bicycle, running, or lifting a weight. As might be expected, the force that can be generated at any given length depends, in addition, on the rate at which the muscle is changing length, its contraction velocity. This is typically characterized by the force-velocity curve for the muscle (Fig. 2.3.13) that expresses the force generated, F , normalized by the force produced under isometric conditions at a given length, F_{max} , as a function of the shortening velocity, v , normalized by the maximum rate of contraction that occurs at zero force, v_{max} . Note that the curve is extended into the range of negative velocities to encompass the case in which the muscle is activated but lengthening since the applied force exceeds F_{max} . When expressed in this dimensionless form, the force-velocity relationship, known as Hill’s equation (McMahon 1984), takes the form:

$$\frac{v}{v_{\max}} = \frac{1 - (F/F_{\max})}{1 + C(F/F_{\max})} \quad (19)$$

where C is a dimensionless constant with values in the range of 4 to 6. Given this relationship between force and the velocity of shortening, we can also compute the normalized power generated by the muscle, which is simply the product of the two:

$$\frac{vF}{v_{\max}F_{\max}} = \frac{1 - (F/F_{\max})}{(F_{\max}/F) + C} \quad (20)$$

As illustrated in Fig. 2.3.13, the normalized power produced by muscle reaches a maximum of about 0.1 when $F/F_{\max} \sim 0.3$. That a maximum exists for an intermediate value of force or shortening velocity simply reflects what we already know from experience, that we can maximize our speed on a bicycle by selecting the appropriate gear.

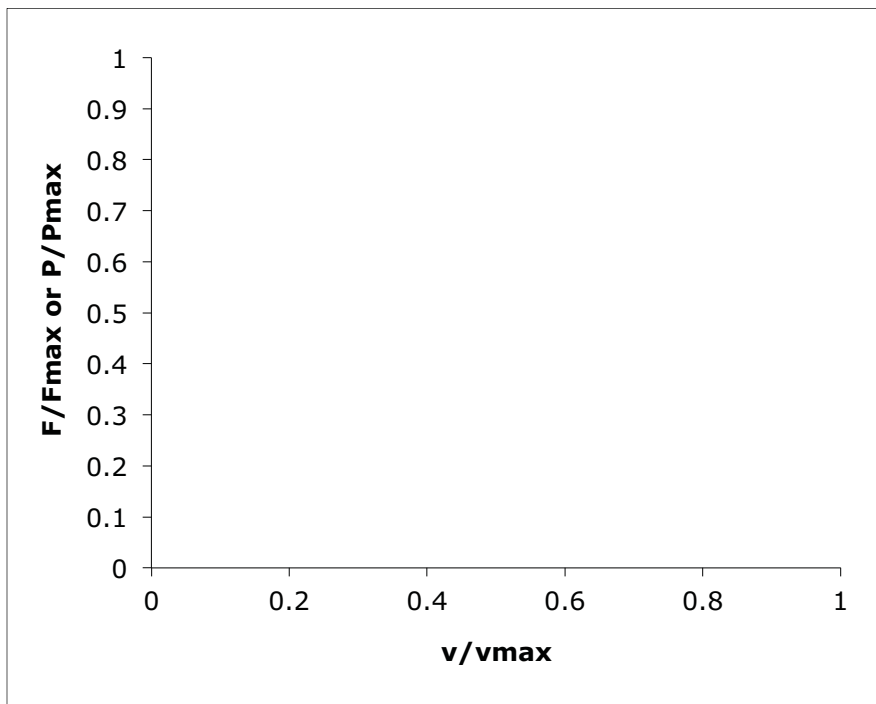


Fig. 2.3.13. Hill's equation (magenta) [in normalized form, eqn. (19)] characterizing the relationship between the force generated by contracting muscle and the speed of contraction. Also shown is the normalized power produced by the muscle (blue) [eqn. (20)], which peaks at a contracting velocity about 25% of the maximum.

Temporal patterns of behavior

All the discussion above pertains to the conditions of maximal stimulus, that is, the condition in which the rate of muscle stimulation is sufficiently high that the muscle is constantly producing the maximum force of which it is capable for the given length and rate of shortening. Obviously, under normal activity skeletal muscle is not always maximally stimulated. Instead, the degree of

muscle activation depends on the rate at which activating impulses are sent to it by the nervous system. The mechanism by which a muscle cell is activated is discussed later in this section; for now, consider the forces produced by the muscle as the rate of stimulus is gradually increased. Consider an experiment in which a single muscle fiber is isolated and mounted at constant length in a system in which the force generated can be monitored over time. If a single activating pulse (electrical stimulus) is applied, the muscle exhibits a single twitch of short duration, lasting on the order of one second (Fig. 2.3.14). If a periodic sequence of pulses is applied, the force builds to a higher level, and oscillates about some mean value. As the rate of stimulation is increased, the mean level of force increases and the magnitude of oscillation decreases, until reaching a state of *tetanus* in which the force achieves a maximum magnitude and the oscillations disappear. In mammalian muscle, tetanus is achieved when the rate of stimulation exceeds about 50 Hz.

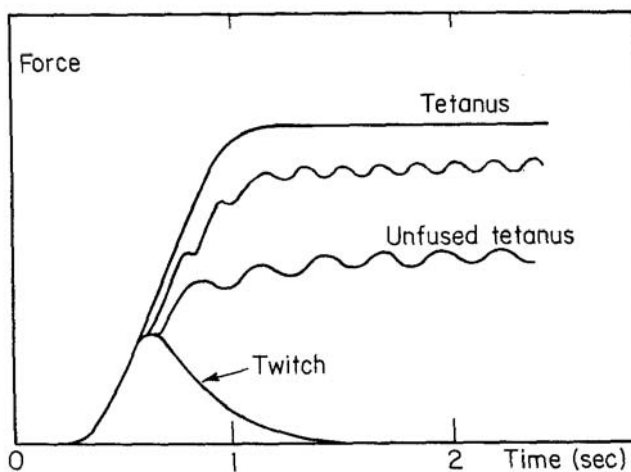
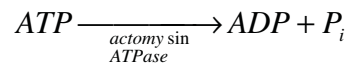


Fig. 2.3.14. Temporal pattern of force generation when a muscle fiber is excited once (twitch), at a low frequency (unfused tetanus), and higher frequencies, eventually producing fused tetanus. [Reproduced from McMahon text.]

The source of energy for muscle

Just as an automobile engine burns hydrocarbon fuel to generate power, muscle, the engine of our body, also extracts power from a chemical reaction. Both do work, and also simultaneously generate heat that must constantly be eliminated while work is being done. The biological fuel that muscles consume to do work is adenosine triphosphate (ATP), and the biochemical reaction that accompanies muscle contraction is the hydrolysis of ATP creating adenosine diphosphate (ADP):

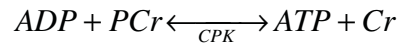


where P_i is the phosphate ion. This reaction has an equilibrium constant, $K_{eq} = 4.9 \times 10^5$ M which strongly favors the production of ADP. This can also be expressed in terms of the change in free energy, ΔG that occurs during the reaction:

$$\Delta G = \Delta G_0 - kT \ln \left(\frac{[ATP]}{[ADP][P_i]} \right) \quad (21)$$

where $\Delta G_0 = -54 \times 10^{-21}$ J (expressed as the change in free energy *per molecule*). At typical concentrations inside the cell, ΔG takes on a value of -101×10^{-21} J or $-25k_B T$.

As ATP is converted to ADP, it is continually being replenished through what is known as the *Lohmann reaction* in which ADP combines with phosphocreatine (PCr) to produce ATP and creatine (Cr):



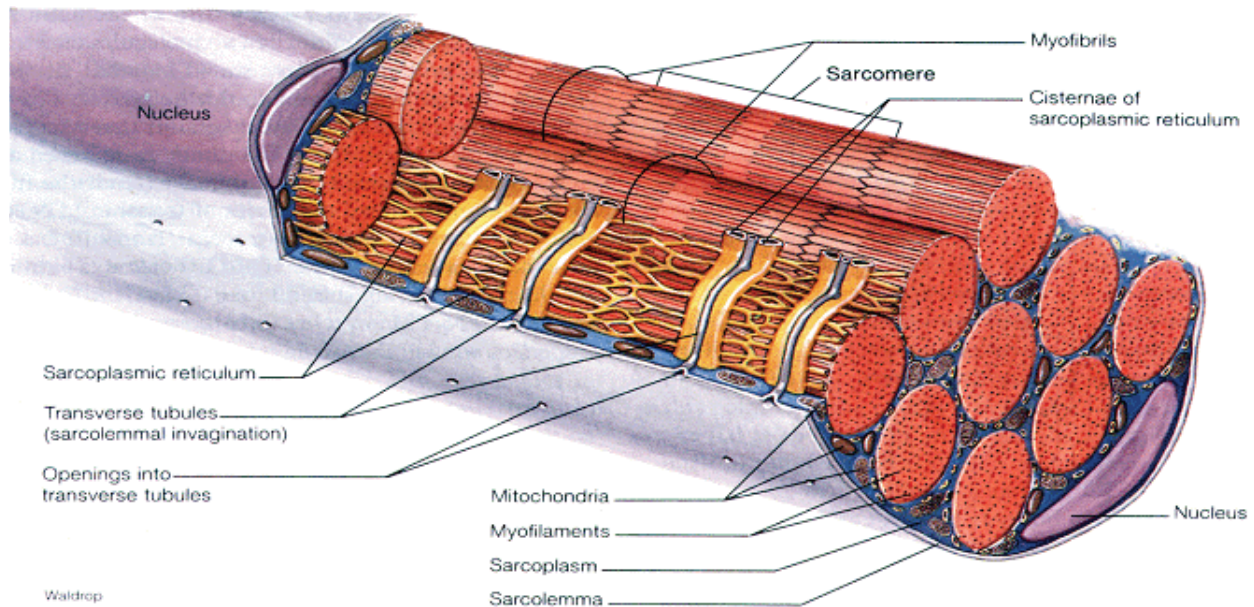
a reaction that is catalyzed by creatine phosphokinase (CPK). The equilibrium constant for this reaction is high, $K_{eq} = 20$, therefore strongly favoring the production of ATP. PCr must also be resynthesized, which is accomplished by a process involving carbohydrates and sugars (Lehninger, Nelson et al. 2000).

When an overall energy balance is performed under a wide range of different experimental conditions, it is observed that the sum of the work done and the heat generated is directly proportional to the rate at which PCr is converted. Thus, it appears that the majority of energy used in muscle contraction is derived from PCr and its reaction with ADP.

Structure of muscle in its various forms

Taking skeletal, striated muscle again as an example, we consider muscle structure starting at the largest length scale, that of the entire functional muscle unit, such as the biceps brachii.

Externally, the muscle attaches to the associated bone via tendons, and its contraction causes the arm to bend at the elbow. Looking at higher magnification, we find that the muscle is actually comprised of a collection of muscle fibers, each of which is a single, multi-nucleated cell about 10-50 μm in diameter that often extend the entire length of the muscle, a distance measured in centimeters. Even at this scale, however, organization at the molecular level begins to become apparent through the striations associated with the sarcomeric structure. These come into clearer view at the next level down in scale; on higher magnification, it can be seen that the muscle fiber



Striated muscle structure from Zubay, et al. Biochemistry 3rd Edition

is comprised of a bundled collection of individual myofibrils, each measuring roughly 1-2 μm in diameter. Here, the sarcomeres can be clearly delineated and the following structures defined (see Fig. 2.3.15):

- *I-band* – a region of low refractive index containing just actin (thin) filaments, divided into two equal parts by the Z-disk, a structural membrane that anchors the actin filaments and runs through the entire muscle fibril.
- *A-band* – a region mostly of higher refractive index that extends the entire length of the myosin (thick) filaments and including a region of overlapping actin and myosin filaments. The A-band contains the H-zone and the M-line.
- *H-zone* – the portion of the A-band in which only myosin filaments are found, containing the M-line where myosin filaments are structurally linked to each other.

The total length of a sarcomere is about 2 μm at rest but varies, as will be seen below, as the muscle shortens or lengthens.

Actin and myosin filaments constitute the molecular motors of muscle. Actin filaments are comprised of *f-actin*, a double helical actin filament of the type found in the cytoskeleton. Thick filaments are made from myosin and arranged in such a way that their long tails merge with the main filament so that the head domains are sticking out, enabling them to interact with the actin filaments. When viewed in cross-section, at a position where the thick and thin

filaments overlap, the pattern consists of a centrally located myosin thick filament, surrounded by **xx** actin thin filaments. Electron micrographs also show the myosin heads bonding with the actin filament at specific binding sites. For a complete description of the molecular structures of actin and myosin, see Section 1 and Chapter 2.2.

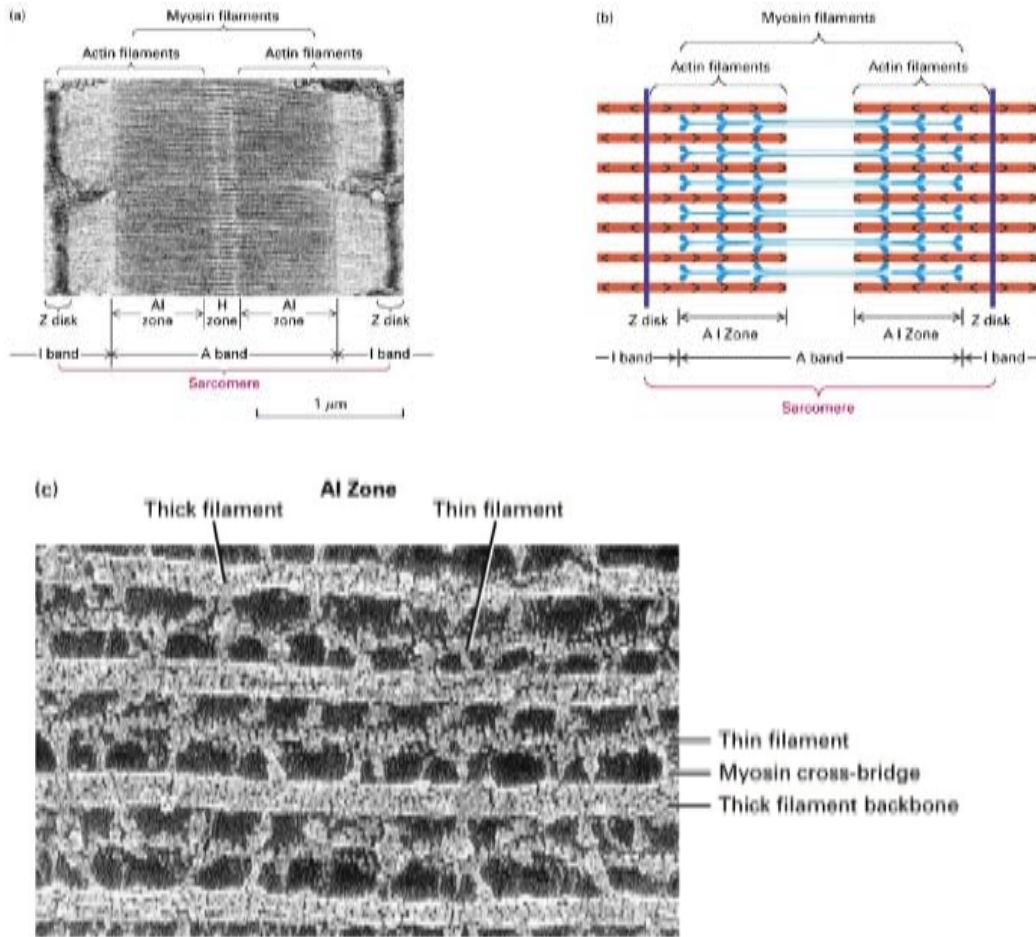


Fig. 2.3.15. Structure of sarcomeres within a muscle cell. (a) Electron micrograph. (b) Sketch showing the relative arrangement of the actin and myosin filaments within a sarcomere. (c) A higher magnification TEM showing the myosin cross bridges spanning between the actin thin filament and myosin thick filament (Reproduced from Lodish et al).

Cardiac muscle is also striated, but the contractile cells (*myocytes*) are shorter and contain a single nucleus. They attach to and communicate with neighboring myocytes through structures called *inter-calated discs* to produce a coordinated, synchronous contraction, initiated, as in skeletal muscle, by a release of Ca^{2+} . *Smooth muscle* is a more primitive form and differs from both skeletal and cardiac muscle by the absence of striations. These single nucleated cells

are spindle-like in appearance, but are less ordered in their arrangement. Contraction occurs more gradually, but can lead to greater overall levels of shortening.

Muscle activation

Calcium ions (Ca^{2+}) provide the molecular trigger that initiates muscle contraction. At rest in a non-activated muscle fiber, Ca^{2+} is primarily contained in the sarcoplasmic reticulum, consisting of two parts, the longitudinal tubules and the transverse tubules, which are actually extended invaginations of the outer membrane. Longitudinal tubules run largely parallel to the sarcomeres, but expand into larger sacs or bulges in the vicinity of the Z-line. Muscle stimulation depolarizes the sarcolemma (the outer membrane of the muscle fiber), which causes a sudden increase in the permeability of the longitudinal tubules, releasing Ca^{2+} into the sarcoplasm to promote actin-myosin interactions.

Calcium initiates contraction through the action of the troponin complex consisting of troponins T, I and C (Troponin-binding, Inhibitory, and Calcium-binding, respectively). When both troponins I and T are bound to actin, myosin is inhibited from binding whether or not Ca^{2+} is present. But with the addition of troponin C, binding to Ca^{2+} releases the inhibition and actin-myosin binding can readily occur with a high affinity.

Soon after contraction is initiated, Ca^{2+} concentration is rapidly brought back to initial resting levels as calcium ions are taken up by the sarcoplasmic reticulum. The Ca^{2+} ion spike typically precedes contraction.

The sliding filament model

Binding of the troponin complex to actin, coupled with an ample supply of Ca^{2+} released from the sarcoplasmic reticulum, sets the stage for muscle contraction and force generation. This is accomplished by means of a relative sliding motion between the actin and myosin filaments during which the myosin heads periodically attach to and are released from binding sites on the actin filaments. The history of this discovery is a fascinating story. It was in 1954 that Andrew Huxley and Ralph Niedergerke (Huxley and Niedergerke 1954), and Hugh Huxley and Jean Hanson (Huxley and Hanson 1954) simultaneously, but independently, published papers in the journal *Nature* describing what has now come to be known as the *sliding filament model* of muscle contraction. In their theory, now supported by a still growing body of work, they proposed the general structure of muscle as depicted in Fig. 2.3.15(b), and described for the first time the arrangement of the actin and myosin filaments and their relative movement during muscle contraction. Through extensions to this theory, it has become clear that the myosin head protruding from the thick filament sequentially binds with the actin thin filament, changes

conformation producing a net relative motion between the filaments, detaches, finally returning to its initial conformation to begin another cycle with a different actin binding site. This is a process repeated over and over again, producing a net progressive displacement or sliding motion between the actin and myosin filaments.

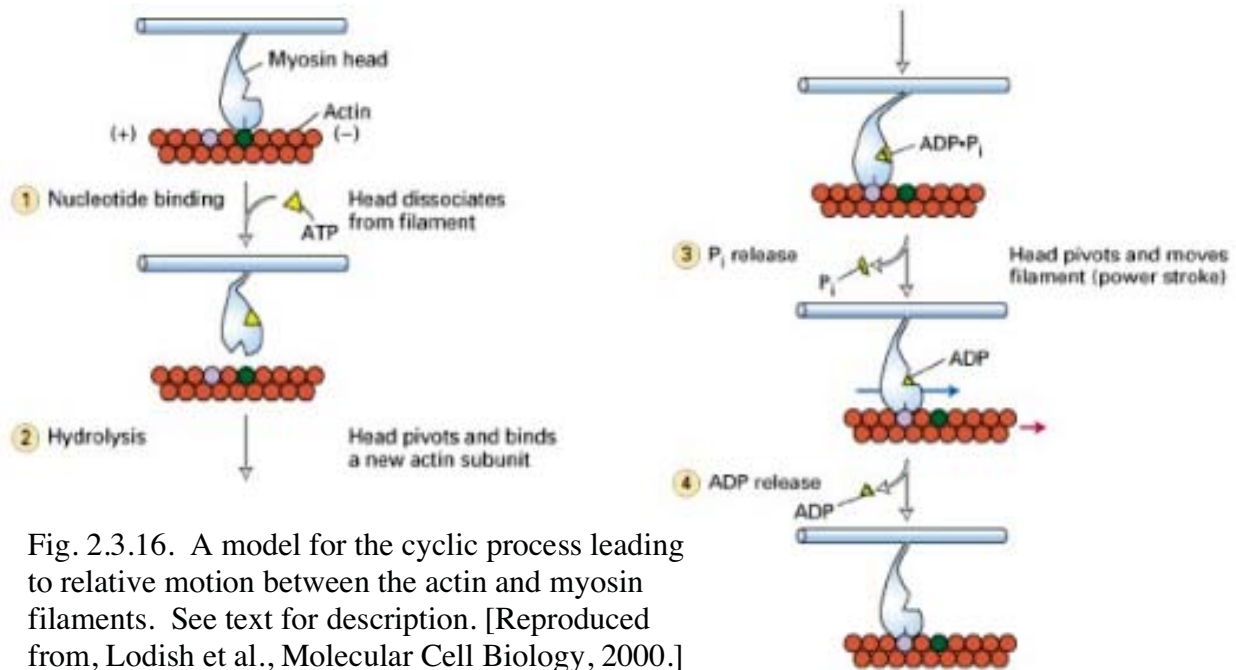


Fig. 2.3.16. A model for the cyclic process leading to relative motion between the actin and myosin filaments. See text for description. [Reproduced from, Lodish et al., Molecular Cell Biology, 2000.]

To better appreciate this process, consider the sequence of events depicted in Fig. 2.3.16, beginning at a point in the cycle where a myosin head is tightly bound to an adjacent actin filament. Before long, ATP binds to myosin, and a conformational change reduces the affinity of myosin to actin and the two separate, simultaneously causing the myosin to shift a distance of about 5 nm toward the positive end of the actin filament during the power stroke where it rebinds at a new location. Hydrolysis then causes the release of one phosphate ion from the ATP (producing ADP) and the associated conformational change triggers the power stroke that drives the actin filament in the direction of its negative end, generating a force that can be as high as 1.5 pN at zero velocity. During the power stroke, the ADP is released returning the myosin to its original state, ready for the next ATP to come along and bind. In fact, each myosin only spends a relatively small fraction of its time bound to actin, even during active muscle contraction. This is made possible by the fact that each actin and myosin filaments have multiple sites of interaction so that even though many sites are free at any given instant, the contraction continues due to the fraction that happen to be attached at that time.

A quantitative model for cross bridge dynamics

A few years after the sliding filament model was proposed, in 1957, A. Huxley published another paper in which he presented a quantitative model for cross bridge dynamics (Huxley 1957).

Though subject to some minor modifications over the years, this model is still widely used to describe the macroscopic behavior of muscle from a molecular perspective. Here we present a slightly modified version of the original model of Huxley, drawing from the presentations of T. McMahon (McMahon 1984) and J. Howard (Howard 2001).

Certain assumptions are made in order to make the problem tractable:

- While in the bound state, the myosin head behaves as though loaded by linear springs with spring constant, κ , and that it passes through the necessary biochemical processes including binding of ATP, ATP hydrolysis, and release of ADP.
- Only the case of constant (time-invariant) relative sliding velocity and force generation is considered.
- The muscle is assumed to be maximally activated throughout.
- Attachment and detachment is assumed to obey simple kinetics.
- Effects of other elastic components in the muscle are ignored.

Following these assumptions, we begin by considering a single myosin head and its interaction with a single actin filament (Fig. 2.3.17), noting that the nomenclature used here is summarized at the end of the chapter. As pictured, the myosin head binding site is attached to springs having a combined spring constant κ , the resting (zero force) position of which is at $x = 0$. When the myosin and actin are bound and the position of the complex is x , the force acting is κx to the left

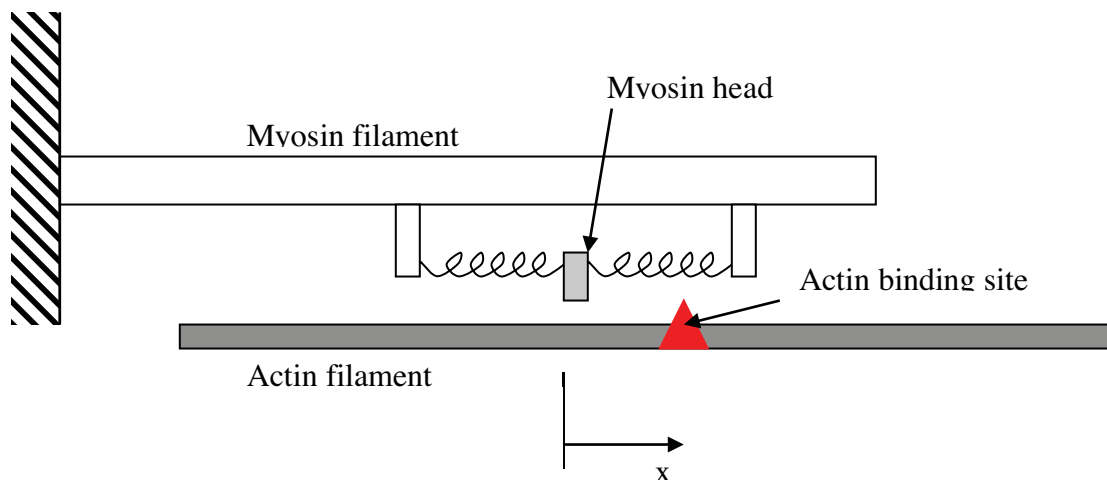


Fig. 2.3.17. Schematic used for the model of cross-bridge dynamics. As the actin filament moves past the myosin filament, the myosin head can bind to it at the red triangle. When it does, the springs are either stretched or compressed and a force κx acts at the binding site.

and the power stroke consists of the complex moving from a position $x = h$ where binding first occurs, to some value of $x \leq 0$ where the two detach. Therefore, for values of $x < h$, the probability that a given cross bridge is attached, $n(x)$, is governed by the rate equation:

$$\frac{dn(x,t)}{dt} = \frac{\partial n(x,t)}{\partial t} - v \frac{\partial n(x,t)}{\partial x} = [1 - n(x,t)]k_+(x) - n(x,t)k_-(x) \quad (22)$$

expressed here in general, time-dependent form, explicitly recognizing that $n(x,t)$ can change either due to the formation of new bonds (first term on the RHS) or the detachment of existing ones (second term), and where $-v = dx/dt$. Since we are interested in the steady state in which $n = n(x)$, this can be re-written as:

$$-v \frac{dn(x)}{dx} = [1 - n(x)]k_+(x) - n(x)k_-(x) \quad (23)$$

which requires forms for the rate constants $k_+(x)$ and $k_-(x)$ for solution. To simplify the analysis, we use the forms suggested by Pate et al. (Pate, White et al. 1993) in which $k_-(x) = k_-^0 = \text{const.}$ for $x < 0$ and zero elsewhere, and $k_+(x) = k_+^0 = \text{const.}$ for $h-x_0 < x < h$ and zero elsewhere (see figure). This equation therefore describes the situation in which a free actin binding site approaches from the right, encounters a myosin head that it may or may not bind to over the short distance x_0 . If it attaches, it remains so during the time that the bonded complex travels leftward a distance h to the position $x = 0$. As it passes into the region $x < 0$, it for the first time has an opportunity to detach and the probability of attachment, $n(x)$, progressively falls, approaching zero in the limit of large negative values of x . Using these forms for the rate constants, $n(x)$ is determined by solution of Eqn. (23) in four distinct regions:

$x > h$:

In this region the actin-binding site is approaching the free myosin head, unoccupied. Since both k_+ and k_- are zero, no binding occurs:

$$n(x) = n(h) = 0 \quad (24)$$

$h-x_0 < x < h$:

If binding is to occur, it has to do so, according to the present simple model, within this narrow region where the binding rate constant is large, described by the equation:

$x < 0$

As the complex moves into the region $x < 0$, the force of interaction sustained at the actin-myosin bond changes sign and its probability of attachment begins to fall, as described by the equation:

$$-v \frac{dn}{dx} = -k_-^0 n \quad (29)$$

Isolating terms in n on the LHS and integrating between x and 0 :

$$\int_{n(x)}^{n(0)} \frac{dn}{n} = \int_x^0 \frac{k_-^0}{v} dx \quad (30)$$

we obtain the solution:

$$n(x) = n(0) \exp\left(\frac{k_-^0 x}{v}\right) = \left[1 - \exp\left(-\frac{k_+^0 x_0}{v}\right)\right] \exp\left(\frac{k_-^0 x}{v}\right) \quad (31)$$

after some reorganization and using Eqn. (27) for $n(0)$.

Equations (24), (28), and (31) provide us with the information necessary to compute the work done in contraction, the force-velocity relationship, and the expressions for maximum generated force and maximum velocity; in short, many of the characteristics features of muscle on the macroscale presented earlier in this section.

Consider first the net work done by a cross bridge that attaches at position $x = a$ and releases at position $x = -b$:

$$W = \int_{-b}^a \kappa x dx = \frac{\kappa}{2} (a^2 - b^2) \quad (32)$$

If we generalize this to the present situation, we need to account for the probability distribution that a bond exists, effectively summing up the work done by each of the individual actin/myosin interactions. In doing so, we seek an expression for the work done by a segment of muscle corresponding to half the length of a single sarcomere ($s/2$), that shortens a distance l , taken to be the distance between sites along a thick filament where actin-myosin binding can occur; l is chosen in this way so that each cross-bridge has the opportunity to go through just a single cycle. Therefore, the work done by this segment, of cross-sectional area A , contracting at constant total force σA is:

$$\sigma l A = \int_{-\infty}^{\infty} [n(x) \rho_s A s / 2] \kappa x dx \quad (33)$$

where ρ_s is the density of cross-bridges (#/volume). It is useful to solve this for the force being generated per unit area:

$$\sigma = \frac{\rho_s A s \kappa}{2 l A} \int_{-\infty}^{\infty} n(x) x dx = \frac{\rho_s A s \kappa}{2 l A} \left[\int_{-\infty}^0 n(0) x \exp\left(\frac{k_-^0 x}{v}\right) dx + \int_0^h n(0) x dx \right] \quad (34)$$

which, when integrated, produces the following useful stress-velocity relationship:

$$\sigma = \frac{\rho_s \kappa s h^2}{4 l} \left[1 - 2 \left(\frac{v}{h k_-^0} \right)^2 \right] \left[1 - \exp\left(-\frac{k_+^0 x_0}{v}\right) \right] \quad (35)$$

Note that this is now an equation that describes the macroscopic behavior of muscle, which was entirely derived from a model of the individual actin-myosin interactions at the molecular scale. It is similar in form to the expression obtained originally by A. Huxley, and as he demonstrated, despite the different algebraic form, can be fit to the experimental measurements made on muscle, previously described as Hill's equation [see eqn. (19)]. For purposes of comparison and to cast this result in a more convenient dimensionless form, we can use eqn. (35) to find expressions for the maximum force generated, obtained by setting shortening velocity v to zero:

$$\sigma_{\max} = \frac{\rho_s \kappa s h^2}{4 l} \quad (36)$$

or, alternatively, the maximum shortening velocity, by setting the stress σ to zero:

$$v_{\max} = \frac{h k_-^0}{\sqrt{2}} \quad (37)$$

Values for v_{\max} are in the range of 6 $\mu\text{m/s}$, so if we choose a reasonable value for h of about 4 nm, $k_-^0 \approx 2000 \text{ s}^{-1}$. As mentioned above, the maximum force in a single cross-bridge is approximately 1.5 pN.

Introducing these as normalizing factors into eqn. (35), we obtain:

$$\frac{\sigma}{\sigma_{\max}} = \frac{F}{F_{\max}} = \left[1 - \left(\frac{v}{v_{\max}} \right)^2 \right] \left[1 - \exp\left(-\frac{k_+^0 x_0}{v} \right) \right] \quad (38)$$

Although this appears to have a very different algebraic form from Hill's equation [eqn. (19)], it is straightforward to show that by proper selection of the parameters, the microscale prediction can be made to agree quite closely with the previous empirically based result (Fig. 2.3.18). Note that in this dimensionless form, only one dimensionless parameter, $k_+^0 x_0 / v_{\max}$ needs to be

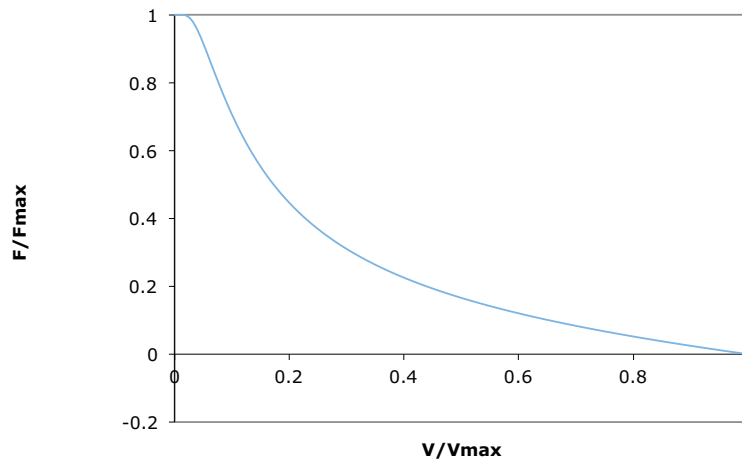


Fig. 2.3.18. Prediction of eqn. (38) with $k_+^0 x_0 / v_{\max} = 0.12$. Note the general agreement with Hill's equation, plotted in Fig. 2.3.13 and given in eqn. (19).

2.3.6 Mechanotransduction in sensory cells

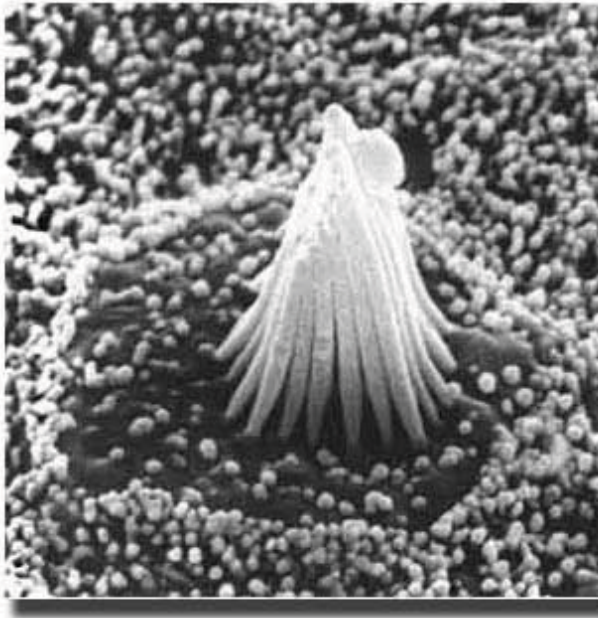
Biological response of cells to mechanical stress

The term "mechanotransduction" has come to denote a spectrum of events from the initial mechanical stimulus of the cell, to the transduction of the stimulus into a biochemical signal, to the signaling cascade that transmits the signal throughout the cell, and through to the end products of this sequence of events, be it a change in gene expression, altered protein synthesis, or changes in cell morphology. Here we take a somewhat narrower view and use the more circumspect definition of "transduction", taking it to be the event that transduces the mechanical perturbation into a change in concentration of some chemical species. While obviously at the heart of all mechanotransduction processes, this step is also arguably the least well understood. Here we describe what is known, largely in the context of sensory perception, but also include some more speculative ideas relating to the response of non-sensory cells. We have come to appreciate over time, that virtually all nucleated cells possess the capability to respond to mechanical force. What we do not yet fully understand, however, is the physical basis for the response, nor the extent to which different types of cells respond through similar mechanisms.

Sensory cells

Hearing is perhaps the most-studied, and most completely understood, example of how cells can respond to a mechanical stimulus. The picture that has emerged from these studies is of a system with exquisite sensitivity and a remarkable range. Sound with energy levels as low of 4×10^{-21} J, (sound pressure levels of about 2.5×10^{-5} Pa) comparable to thermal noise, can be detected by the human ear, as well as sounds with intensities 13 orders of magnitude times as large (!), at the threshold of pain. Spectral sensitivity in humans ranges from 20 Hz to 20,000 Hz, and even wider ranges are sensed by other species.

Sound is transmitted in the form of vibrations from the tympanic membrane, via the ossicles of the middle ear (hammer, anvil and stirrup), ultimately producing oscillations in the oval window. These, in turn, excite waves of fluid motion that propagate through a snail-shell shaped structure called the cochlea. In cross-section, the cochlea can be seen to be comprised of three chambers, the central one being the cochlear duct that contains the organ of corti (Fig. 2.3.19). Transduction of mechanical motion into a biochemical, then electrical signal occurs at the level of the stereocilia present in individual hair cells that reside in the organ of corti and respond to the motion of the basilar and tectoral membranes as waves propagate down the liquid-filled channels of the cochlea. Stereocilia are actin-filled microvilli that organize into a cone-shaped bundle (Fig. 2.3.19) and can extend up to 30 μm from the cell surface.



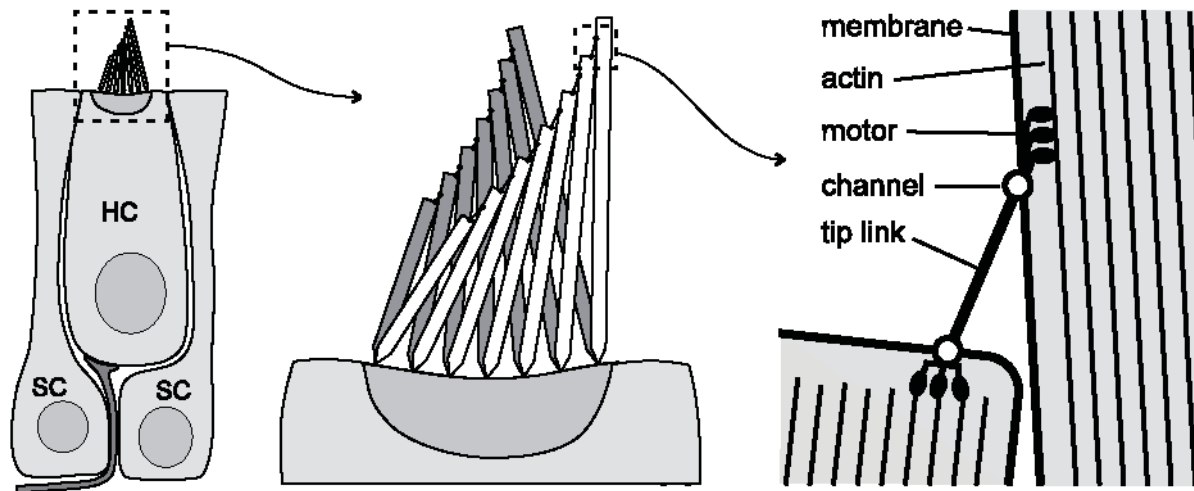


Fig. 2.3.19. Top: A collection of stereocilia extending from the surface of a single hair cell. The resulting bundle extends about $30\ \mu\text{m}$ from the cell surface. [Reproduced from [Hudspeth](#) website.] Bottom: How a force acting on two neighboring stereocilia gives rise to an increased tension in the tip link. The tip link is thought to attach to a stretch-activated channel at one or both ends so that an increase in tip link tension activates the channel(s). [Reproduced from Garcia-Anoveros & Corey, *Ann Rev Neurosci*, 1997.]

Sound is transduced in the hair bundle by the opening of stretch-activated potassium channels along the stereocilia caused by a shearing displacement of one stereocilium relative to another (Fig. 2.3.19). Relative motion produced by shearing induces a force in thin filaments that connect the tip of one stereocilium to a gated channel in its neighbor. This presumably leads to a conformational change in the transmembrane protein that comprises the channel, causing it to open. Measurements suggest that the force required to open the channel is only about $2\ \text{pN}$, corresponding to a displacement at the channel of about $4\ \text{nm}$ ([Hudspeth](#)).

Opening of the channel can be viewed as a transition between two ensembles of conformational states, or *structural states*, corresponding to the open (1) and closed (2) conditions. Since each structural state (open or closed) can have a number of conformational states, the transition between structural states must be analyzed in terms of the difference in free energy $G = U - TS$ where U is the average potential energy of the *ensemble* of conformational states in a single structural state and S is its entropy. It can be shown that the probability of existing in one structural state or another also satisfies Boltzmann's law, so that

$$P_i = \frac{\exp(G_i / k_B T)}{\sum_i \exp(G_i / k_B T)} \quad (39)$$

So that the ratio of probabilities is

$$\frac{p_2}{p_1} = \exp\left[-\frac{\Delta G}{k_B T}\right] \quad (40)$$

taking p_1 and p_2 to be the closed and open states, respectively, and ΔG the difference in free energy between them. If the transition from closed to open states corresponds to a movement of distance Δx along the direction in which the force F acts, then the difference in free energy between the two states is:

$$\Delta G \cong \Delta G^0 - F\Delta x \quad (41)$$

where ΔG^0 corresponds to the difference in free energy between states without an external force. Recognizing that the channel is either open or closed, so that $p_1 = 1 - p_2$, and letting K_{eq}^0 be the equilibrium constant in the absence of force, we can write:

$$\frac{p_2}{1 - p_2} = K_{eq}^0 \exp\left[\frac{F\Delta x}{k_B T}\right] \quad (42)$$

and when solved for the probability that the channel is open:

$$p_2 = \frac{1}{1 + \frac{1}{K_{eq}^0} \exp\left[-\frac{F\Delta x}{k_B T}\right]} \quad (43)$$

Assuming the channel is normally closed, $K_{eq}^0 \ll 1$, so that $p_2 \rightarrow 0$ with no force applied, the channel behavior is as shown in Fig. 2.3.20. Values for Δx are thought to lie in the range of 2 to 4 nm, so the force required to fully open the channel is about 10-20 pN.

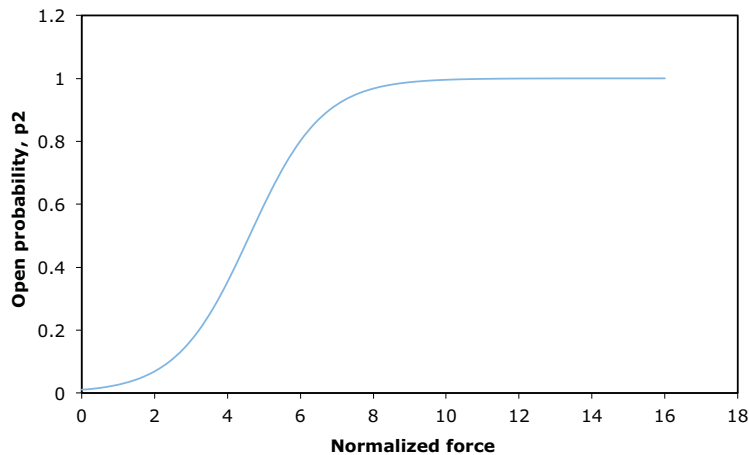


Fig. 2.3.20. The change in probability that the channel is in the open state as normalized force, $F\Delta x/(k_B T)$ is varied. In this example, K_{eq}^0 was arbitrarily set to 0.01, but the curve is relatively insensitive to this value provided it is small.

2.3.7 Mechanotransduction in non-sensory cells

While the need for mechanotransduction is obvious in the case of sensory cells, it is less so in the case of other, non-sensory cell types. Nonetheless, we now know that nearly every type of cell has the innate capability to respond to a mechanical stimulus. Many of the cells' responses contribute to normal physiologic function. As one example, when a cell is exposed to higher levels of stress from its environment, it typically responds by increasing its own stiffness by remodeling its cytoskeleton, increasing its strength of adhesion to surrounding structures, and often by upregulating the synthesis of extracellular matrix proteins. All this tends to make the cell better able to withstand the imposed stress and resist damage. On a larger scale, the coordinated response of the cells contained in the wall of an artery, provide the means for the vessel to adjust to changes in the level of flow or changes in pressure. In the former case, a reduction in flow, for example, leading to a reduction in wall shear stress, elicits a response from the resident cells – endothelium, smooth muscle cells, and fibroblasts – that lead to wall remodeling and a subsequent reduction in vessel diameter. Through this response, the arterial system maintains vascular dimensions appropriate for the distribution of blood flow. This same response, however, can contribute to pathologies as in the case of atherosclerosis. Regions of low wall shear stress in bifurcations, for example, experience the same tendencies for vessel narrowing, which, in combination with other biological responses, can ultimately lead to

localized constrictions and flow impairment. Thus, a healthy, desirable response contributes to the disease process in the long term. Numerous other examples could be given: bone remodeling due to stress, the stimulation of collagen and glycosaminoglycan synthesis by chondrocytes in cartilage. Many of these processes play major roles both in tissue repair or remodeling and the progression of disease. For these reasons, the study of cellular responses to mechanical force has become a major effort and continues to be a focus in many research laboratories.

Physical factors that elicit a response

Cells are subjected to a variety of forces during the course of normal function, and these forces vary considerably both in magnitude and in time-course. For example, cartilage and bone experience stresses in the range of several MPa during normal function, and as high as 10^3 of MPa in extreme situations. Stresses resulting from muscle contraction are in the range of 10^5 Pa. Arterial blood pressure is about 10^4 Pa, and circumferential stresses in the arterial wall are about an order of magnitude higher than that. By contrast, the shear stress exerted on the vascular endothelium is in the range of 1-4 Pa, and the shear stress experienced by a cell settling in plasma under the action of gravity is down around 10^{-3} Pa. Clearly the range of stress in tissue is enormous, spanning more than 10 orders of magnitude! One needs to be careful, however, in relating these figures to the stresses experienced directly by cells. In the case of bone and cartilage, the extracellular matrix supports the vast majority of the stress borne by the tissue. The same is true in the vessels of the circulation. In addition, we need to draw a distinction between hydrostatic pressure (1/3 times the trace of the stress tensor) and the stresses such as shear that cause cellular deformation. This is a point we will return to later, but for now, it is sufficient to recognize that arterial endothelial cells appear to be more sensitive to changes in shear stresses in the range of 1 Pa than to changes in pressure as high as 10^4 Pa. The difference appears to lie in the level of deformation experienced by the cell in each case.

Various types of mechanical stimulus have been implicated in eliciting a biological response (see Table 1). Essentially any manner in which the cell might be subjected to force or experience deformation can elicit a reaction from the cell. While it is often difficult to relate one type of stimulus to another, a common feature of the conditions necessary to produce a response is (1) a level of strain in the range of 1 to 10%, or (2) shear stresses in the range of 1-10 Pa. Noting that the Young's modulus of the cytoskeleton for a typical cell is in the range of 100 Pa, these values for stress and strain can be seen to be roughly equivalent, i.e., a stress of 1-10 Pa applied to a material with a modulus of 100 Pa will produce strains of 1-10%. We might expect, therefore, that cells exhibiting a higher modulus might require either higher levels of stress or

less strain before they respond, depending on whether the critical feature of the stimulus is stress or strain.

It has also been observed that cells respond differently to static stresses or strains than to those applied in a cyclic or more generally time-dependent manner, suggesting that the temporal nature of the load or deformation is critical in determining the threshold, if not the nature, of the response. For example, the magnitude of the response of endothelial cells to shear stress in a laminar shear flow is observed to depend upon the rate at which the shear stress is ramped up with time. Also, the response of a cell to laminar (steady) or turbulent shear stress can be quite different, even if the average value is the same for the two flows. While the basis for this influence of time varying stress has not been identified, a number of possibilities exist. Due to the viscoelastic character of the cell and cell membrane, the deformations associated with a particular level of strain will depend on the frequency of forcing.

Stimulus	Threshold level for response
Fluid dynamic shear stress	0.1-0.5 Pa
Cyclic strain	1%
Osmotic stress	
Compression in a 3D matrix	1-4% strain
Transmembrane stress	0.5 kPa
Perturbations via tethered microbeads	1 nN

Table 1. Physical stimuli known to elicit a biological response.

Methods used to test cellular response

A wide variety of in vitro systems have been employed to apply stress or strain to cells in a controlled manner and thereby test their biological response. These systems can be broadly classified according to whether the level of strain or stress is controlled in the experiment (Table 1). Generally it is desirable that the conditions to which the cells are subjected is uniform, since the common methods for assessing biologic response involves harvesting the entire cell population and using methods such as Northern blots or Western blots to test for mRNA or protein, respectively. Recently, however, new methods have been developed (e.g., in situ

hybridization) that provide information on the distribution of a particular response, thereby precluding the need for uniform stimulus.

The range of conditions used in these systems is typically determined so that the levels of stress or strain exceed the threshold values to elicit a biological response, but fall short of those that cause cell death as, for example, by rupturing the cell membrane. This essentially dictates the ranges shown in Table 2. One of the objectives in their design is to produce a condition that mimics that experienced by cells *in vivo*, yet is simple enough to exert sufficient control and minimize the presence of extraneous, confounding factors. Hence, systems have generally produced either strain or stress, though in some instances an attempt is made to replicate both. One example is in the case when cells are grown on the interior surface of a compliant tube so that the cells experience shear stress and strain simultaneously. Experiments such as these provide a means of studying potential synergistic effects of multiple factors.

Device for applying stress	Range and type of stress or strain	Degree of uniformity in stress magnitude	References
parallel flow chamber	shear, 1-100 Pa	uniform, except near entrance	
cone-and-plate viscometer	shear, 1-100 Pa	uniform	
radial flow chamber	shear, 1-100 Pa	varies as 1/r	
biaxial stretch, bulging membrane	strain, 1-20%	non-uniform	
biaxial stretch, oscillating cylinder	strain, 1-20%	uniform	
compliant tube	strain + stress	uniform stress, except near entrance, axial strain different from circ. strain	
confined compression in 3D matrix	strain	uniform in direction of compression	
unconfined compression in 3D matrix	strain	non-uniform	
tethered microbeads	force (1-10 nN??) or displacement (1-5 μm)	non-uniform, but localized	
hydrostatic pressure	pressure, up to 1 atm	uniform	
transmembrane pressure	pressure differential, (<3000 Pa)	uniform	

Table 2. Experimental systems used to investigate the biological response of cells in culture to a mechanical stimulus.

Types of response

When one considers the enormous body of literature devoted to mechanotransduction, it is difficult to discern the underlying threads that tie it all together. There exist many ways in which to characterize the complexities of the response of a cell to mechanical stimulus – here we consider two perspectives: (i) in terms of the time-course of the biological response involved, and (ii) in terms of the fundamental cellular function targeted by the collective response (e.g., how is the response manifested with regard to the fundamental workings of the cell such as migration, differentiation, division, etc.).

These classifications require some elaboration. For the first, we can think in terms of the sequence of events leading to the different types of response (see Fig. 2.3.21). As the term, *signaling cascade*, implies, the response occurs in a sequential manner, beginning with events immediately following transduction, within seconds of the mechanical stimulus, but often taking hours, days, or even longer to achieve the end result. For example, the sudden onset of fluid shear stress gives rise to an almost immediate increase in calcium ion concentration – within a period of about a minute. Some of the responses are even more rapid, as can be seen in Fig. 2.3.21. Other responses take somewhat longer and involve a signaling pathway, but one that is confined to the cytoplasm and does not involve changes in gene expression. These responses typically take longer, from minutes to hours, and are often localized. Examples include the changes in cytoskeletal structure that occur in the vicinity of the mechanical stimulus, as by an adherent bead forced by a magnetic trap. The third category includes all those responses mediated by changes in gene expression and altered protein synthesis. These typically take longer, on the scale of hours, but also produce the greatest long-term effects. For example, changes in the rates of production of extracellular matrix molecules will, over a long period, lead to interstitial remodeling. The entire remodeling process may take weeks or even years. Finally, there may be responses that influence post-translational modification of synthesized proteins. These may occur entirely in the cytoplasm, independent of any nuclear events.

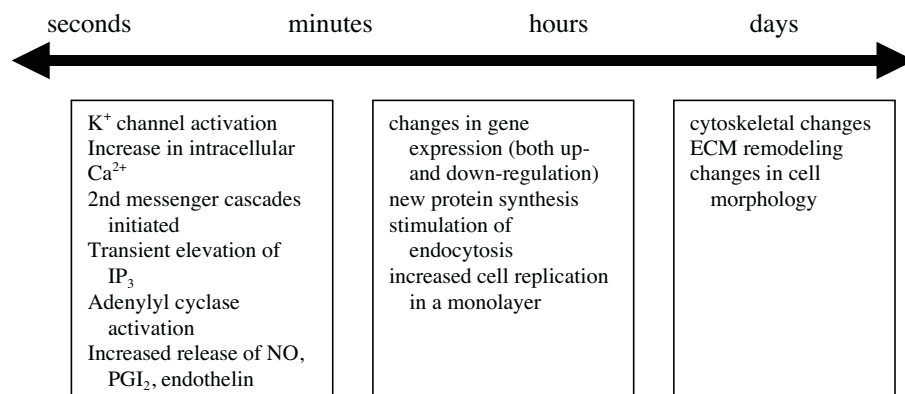


Fig. 2.3.21. Some examples of the time-scale for the biological response of a cell.

**Some Selected Functional Consequences
of Mechanical Stimulation**

Changes in endothelial cell morphology
Reorientation and migration of connective tissue cells
Extracellular matrix remodeling
Thrombus formation
Increased rate of mitosis when stretched
Altered chemotactic response
Changes in the rate of endocytosis
Arterial vasoconstriction
Change in cell phenotype
Growth of stretched nerve axons
Production of more actin and myosin by muscle cells

Table 3. Examples of biological functions that are known to be influenced by mechanical stimulus.

The second way in which we can characterize the response, as mentioned above, is in terms of the end effect. One of the processes influenced by mechanical stimulus is cell migration. But migration involves a multitude of responses that collectively lead to the observed change in motility. This might include polarization of the cell, changes in the rate at which various cytoskeletal proteins are synthesized, changes in the synthesis and release of enzymes to degrade the extracellular matrix; collectively this represents a change in phenotype from a stationary to migratory cell. Other types of collective response are listed in Table 3.

Often the rational basis for the collective response is not immediately apparent. In the case of the changes in cell alignment and morphology in response to laminar fluid dynamic shear stress (see Fig. 2.3.22), it took years after the initial observation before it was realized that at least one consequence was to reduce the drag experienced by the cell. Cells are also observed to reorient in response to cyclic strain. If the strain is uni-directional, for example, the cells become elongated with their long axis pointing in a direction perpendicular to the axis of deformation (Ives, Eskin et al. 1986); this coincides with the development of actin stress fibers (bundles of actin filaments) similarly aligned (Sumpio, Banes et al. 1988).

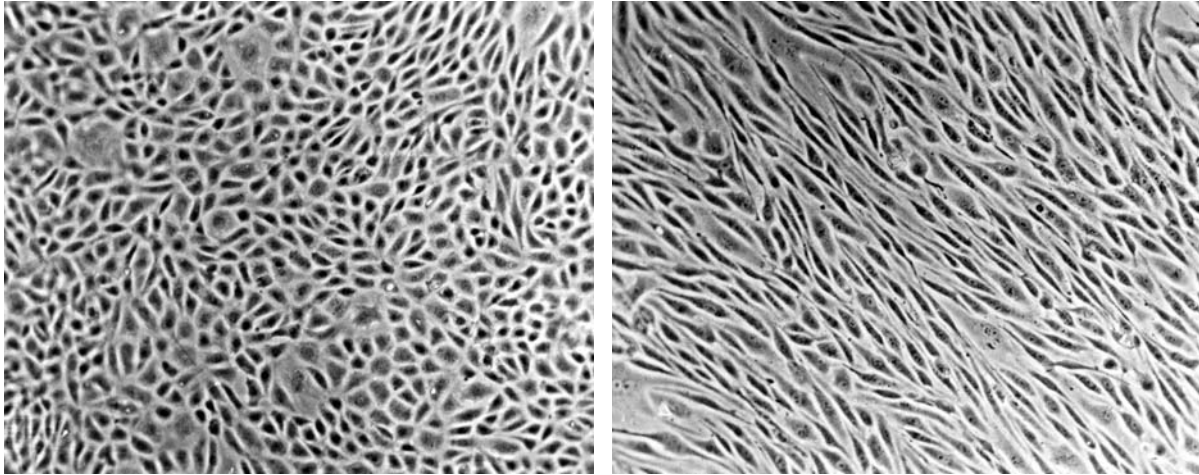


Fig. 2.3.22. Phase contrast micrograph showing the alignment of bovine aortic endothelial cells in the direction of flow as seen in cell culture subjected for 48 hr to either no flow (static) conditions (a) or a steady, laminar shear of 0.8 Pa; flow from upper left to lower right (b). [Reproduced from (Dewey, Bussolari et al. 1981).]

Current theories of mechanotransduction

Although we currently have little detailed understanding of how cells sense a mechanical stimulus, this is an active area of research and advances are sure to come. At present, we have a reasonably complete picture of how one stretch-activated ion channel changes its conductance in response to changes in tension in the lipid bilayer. We also know to some degree of detail how hair cells in the ear respond to mechanical perturbation. In most other cases, however, particularly in the case of non-sensory cells, theories have been proposed, but they await experimental confirmation. Here we begin with a discussion of stretch-activated channels and use this as a basis for the discussion of other, less well understood, theories of mechanotransduction.

Stretch-activated or mechanosensitive channels. Some years ago, Nehar, Sakmann and Steinback (The extracellular patch clamp: a method for resolving currents through individual open channels in biological membranes. *Pflugers Arch.* 1978 Jul 18;375(2):219-28.) developed an experimental technique in which a small region of the cell membrane can be isolated and its conductance measured. A micropipette with diameter in the range of 1 to several microns is brought into contact with the cell, and the membrane is drawn into the mouth of the pipette by means of a slightly negative pressure, producing a seal between the pipette and the membrane

and isolated in small region of membrane to which different pressures or different solutions can be applied. This procedure, referred to as a *patch clamp*, provides a means by which the conductivity of the membrane can be measured and has been widely used in ion channel research.

Using the patch clamp technique, it can easily be demonstrated that certain ion channels change their conductivity in response to changes in the level of pressure acting across the membrane. Recall from the Law of Laplace that the membrane tension σ is related to the transmembrane pressure drop Δp through the relationship:

$$\sigma = \frac{R\Delta p}{2} \quad (44)$$

where R is the radius of curvature of the membrane within the mouth of the pipette. Although different channels have been found to respond to different levels of stress, the minimum pressure differences needed to open a channel typically fall in the range of 10 to 100 mmHg (roughly 10^3 - 10^4 Pa) and values of membrane tension necessary to open 50% of the channels have been estimated to be approximately 10^{-2} Pa m. This value falls close to the level of tension at which a lipid bilayer ruptures ($\sim 6 \times 10^{-2}$ Pa m; see Ch. 2.2), supporting the theory that one function of these channels is to allow the free passage of ions out of the cell, preventing membrane rupture in the event of a sudden drop in ambient osmotic pressure.

One of the channels that has been extensively studied is the bacterial mechanosensitive channel (*MscL*, for *Mechano-sensitive channel of Large conductance*). Extensive experimental data using the patch clamp technique have shown that this channel opens at pressures above about 40-60 mmHg, corresponding to a critical level of membrane tension of about 10-12 dyn/cm = $1-1.2 \times 10^{-2}$ Pa m. More importantly, the crystal structure of this channel was recently identified to 3.5 angstrom resolution (Chang, Spencer et al. 1998) (Fig. 2.3.23), and the effects of changes in membrane tension have been numerically simulated using molecular dynamics (Gullingsrud, Kosztin et al. 2001). In these, each individual atom in each molecule contained in the lipid bilayer and channel is simulated, and changes in molecular conformation due to stress in the membrane considered. Results of these simulations show that membrane tensions in the range of those found experimentally to produce an increase in conductance, also produce a significant conformational change in the protein, consistent with the conductance change.

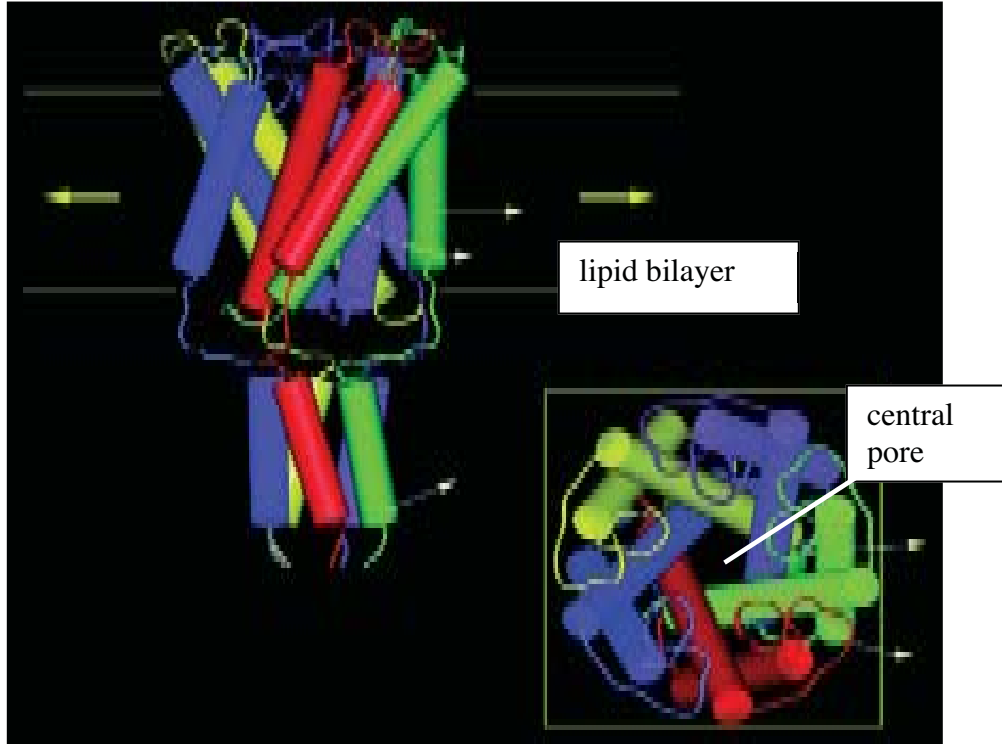


Fig. 2.3.23. Molecular structure of the MscL channel as shown both from the side and looking down the internal pore (inset). Yellow arrows indicate membrane tension [reproduced from (Chang, Spencer et al. 1998)].

Membrane surface tension may not be the only force that can control channel conductivity. Strong evidence suggests that the proteins that comprise other channels may possess direct mechanical linkages to the extracellular matrix and/or the cytoskeleton. In that event, forces transmitted via these linkages to the channel might also produce a conformational change. One example of this type of mechanical linkage has been postulated in hair cell activation, as discussed earlier in this chapter. In this case, forces transmitted via the tip link connecting one stereocilium to another (Fig. 2.3.19) are thought to produce a conformational change in the channel protein, leading to a change in conductance and producing the required stimulus.

Forces transmitted through transmembrane proteins. Various cell surface receptors are used to anchor the cell to its surroundings, as was discussed in the context of cell adhesion in Chapter 2.2. Since many of these proteins serve a structural role, they also provide a means by which forces can be transmitted across the lipid bilayer to the intracellular network. In many cases, the

act of receptor-ligand bonding is, by itself, sufficient to trigger a biochemical reaction on the intracellular side of the membrane and, potentially, to set off a signaling cascade. It has therefore been reasoned that forces transmitted via these same receptors might also produce conformational changes in them, or in the proteins that form the structural link between extracellular and intracellular elements, and lead to a similar sequence of events (Fig. 2.3.25).

The integrin family has often been implicated in such a role because of its importance in cell adhesion and since integrins are well known to act as signaling molecules. Integrins represent some of the primary receptors of extracellular matrix molecules and are known to play a role in cell migration, cytoskeletal rearrangement and a variety of signaling pathways, some of which can also be initiated by mechanical stimulus.

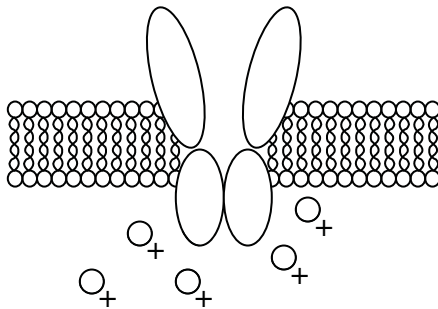
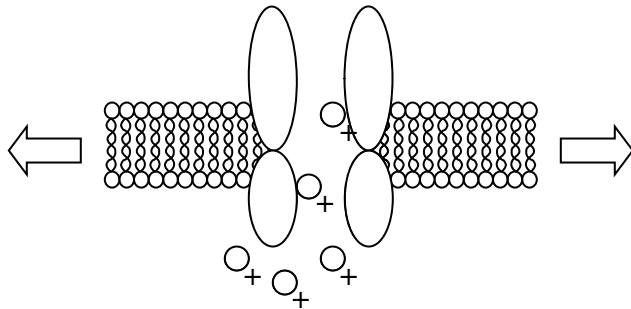


Fig. 2.3.24. A mechanosensitive ion channel in its initial closed position (top) excluding ion exchange, and opened as a result of membrane tension (bottom) allowing small ions to pass freely.



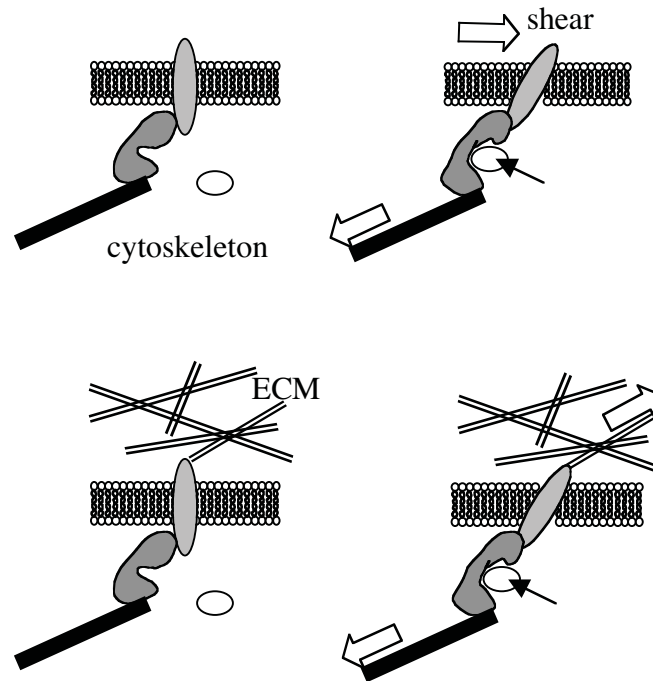


Fig. 2.3.25. Conformational changes in a protein linking a transmembrane receptor to the cytoskeletal network, leading to a reaction on the intracellular side of the membrane. Top: Shear forces due to flow over the cell layer are transmitted via protein linkages to the cytoskeleton. Bottom: Forces originating from the extracellular matrix are transmitted to the cytoskeleton, leading to conformation changes in the linker proteins.

In order to respond in such a way as to initiate a biochemical reaction, the forces applied to a single integrin receptor must be sufficient to produce a conformational change in the intracellular domain of the protein. While we know little about the level of force necessary to accomplish this, it is possible to establish some rough estimates. Studies using atomic force microscopy have shown that a single receptor-ligand bond detaches when a force of between 30 and 100 pN is applied from the extracellular side (Lehenkari and Horton 1999). If an integrin molecule is to act as a force transducer, then it must respond to forces no greater than this.

Proteins typically form into multiple globular regions or *domains* that can be connected by relatively flexible sections that permit twist or a hinge-like motion. Binding sites are often located in the cleft of these hinged regions and thus, the degree to which the hinge swings “open” determines the binding affinity for the appropriate ligand. Movements about this “hinge” occur as a result of forces as small as 0.1 to 1 pN (Bao, G., *Mechanics of Biomolecules*), and therefore can even be influenced by Brownian effects. With the application of higher forces, in the range of 1 to 100 pN, the domains themselves begin to undergo deformation. For example, experiments in which single molecules (e.g., titin and tenascin) are isolated and stretched using a laser trap indicate that forces in the range of 100 pN can be sufficient to unfold individual

domains (Tskhovrebova, Trinick et al. 1997; Oberhauser, Marszalek et al. 1998). While all this is strongly suggestive, there is not yet any direct evidence demonstrating the role of force-induced conformational changes in integrins, or any other intracellular protein, in the transduction of a mechanical to biochemical signal.

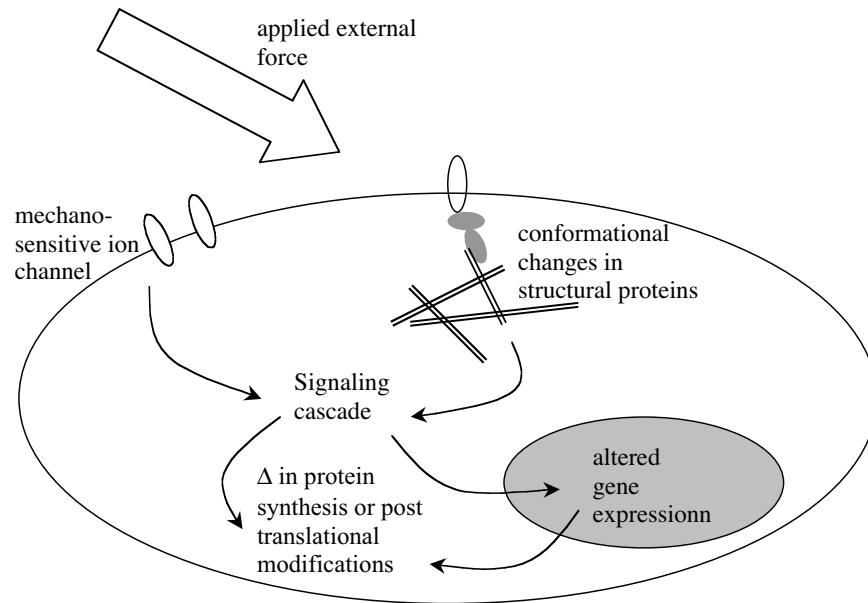


Fig. 2.3.26. Summary of the ways in which a cell responds to external forcing. The applied force is transduced into a biochemical signal, here shown either by activation of a stretch activated (mechano-sensitive) ion channel or by conformational changes in intracellular proteins. This triggers a signaling cascade that can result in changes in gene expression, changes in cytoplasmic processes, or changes in post-translational modifications of protein. Altered gene expression changes the profile of proteins synthesized by the cell.

Mechanotransduction at sites remote from the point of forcing. Forces acting external to a cell are subsequently distributed throughout the cell interior via the cytoskeletal network, leading to the possibility that the site of transduction may be quite remote from the point of stimulus. Although the levels of stress will generally fall with increasing distance from the site of origin, several factors might cause forces to become concentrated at particular remote locations. For example, when the forcing itself is diffuse, the locations of maximum force are more likely to depend on how the cell adheres to its surroundings, and how concentrated or diffuse the adhesion sites are. In focal adhesion complexes, especially common in cells grown in two-dimensional culture and mechanically stimulated, the forces exerted by fluid dynamic shear tend to be

focused, and the forces acting within network structures in the immediate vicinity of the focal adhesion may be among the highest found in the cell.

The impact of this can easily be seen through the following example. Consider an isolated endothelial cell with a surface area of $1000 \mu\text{m}^2$ exposed to steady shear stress of 1 Pa (10 dyn/cm^2), which adheres to the substrate via 50 focal adhesion sites, the average area of each being $4 \mu\text{m}^2$. In order to maintain a force balance, the stress must be amplified 5-fold, to an average of 5 Pa at each adhesion site. Moreover, because the shear stress produces a torque on the cell, forces will not be uniformly distributed; adhesion sites near the upstream end of the cell will need to support a larger force, on average, than those on the downstream end, provided the density of adhesion sites is uniform.

Focusing can also occur at points of cross-linking between cytoskeletal filaments, where large forces or torques might additionally act on individual proteins (Fig. 2.3.27). Stress-related changes in the binding of cytoskeletal proteins have been demonstrated in cells stripped of their lipid bilayer and subjected to strain on an elastic substrate (Sawada and Sheetz 2002), suggesting that deformations of about 10% can lead to selective binding. It is becoming increasingly clear that external forces can alter reaction kinetics within the cell, and that these are likely mediated by conformational changes in individual proteins.

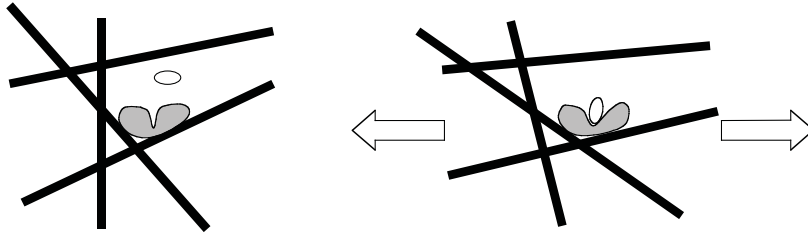


Fig. 2.3.27. Mechanotransduction mediated by proteins that bind to, and possibly cross-link the individual filaments of the cytoskeleton. Stresses applied to the network expose a binding site in the linking protein, allowing a chemical reaction to take place.

Changes in the mobility and aggregation of membrane proteins. Other processes have also been shown to be related to mechanotransduction events. One of these is a reduction in membrane viscosity as a result of the application of fluid dynamic shear stress (Haidekker, L'Heureux et al. 2000). While the events that cause the reduction in membrane viscosity have not yet been elucidated, such a reduction would lead to freer mobility of transmembrane proteins and an increased likelihood of receptor aggregation, thereby affecting their rates of reaction.

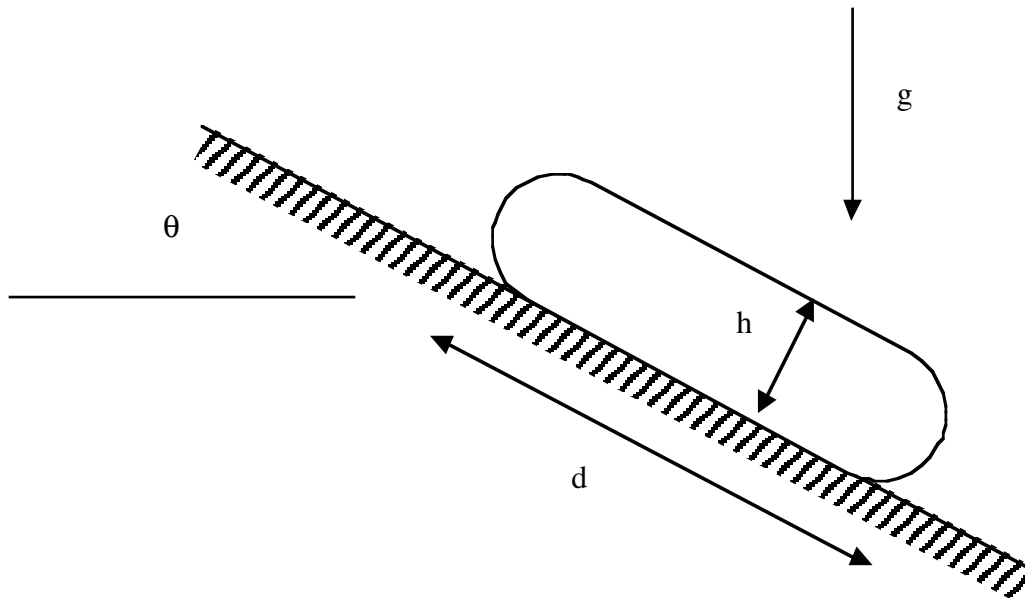
3.3.7 Nomenclature:

x	=	location of actin binding site relative to location of zero force on myosin head
v	=	velocity of actin filament relative to myosin filament
$n(x)$	=	probability of actin-myosin attachment between x and $x+dx$
$k_+(x)$	=	rate constant for actin-myosin attachment
$k_-(x)$	=	rate constant for actin-myosin release
k_+^0	=	constant value for $k_+(x)$ in the range $x < 0$
k_-^0	=	constant value for $k_-(x)$ in the range $h-x_0 < x < h$
h	=	distance between site of attachment and zero force point
x_0	=	distance over which binding occurs ($h \gg x_0$)
ρ_s	=	number of sarcomeres / unit volume
κ	=	spring constant for crossbridge
s	=	sarcomere length
l	=	distance between cross bridges on a sarcomere
F	=	total developed force in a muscle
A	=	cross-sectional area of muscle

3.3.8 Problems

1 -- Gravitationally-driven cell

Consider a highly viscous, non-wetting droplet that slowly slides down an inclined plane under the action of gravity. Obtain a *scaling expression* for the speed at which the droplet ("cell") travels down the plane, as a function of the gravitational constant, g , the density of the droplet, ρ , the angle of inclination, θ , the height of the droplet, h , and the diameter of the contact area (assumed circular), d . You may assume that the droplet takes on the shape of a pancake ($h \ll d$) under the conditions of measurement, and that the result can be obtained by balancing the rate at which work is done by gravity with the rate of internal viscous dissipation.



2 -- Cell Migration

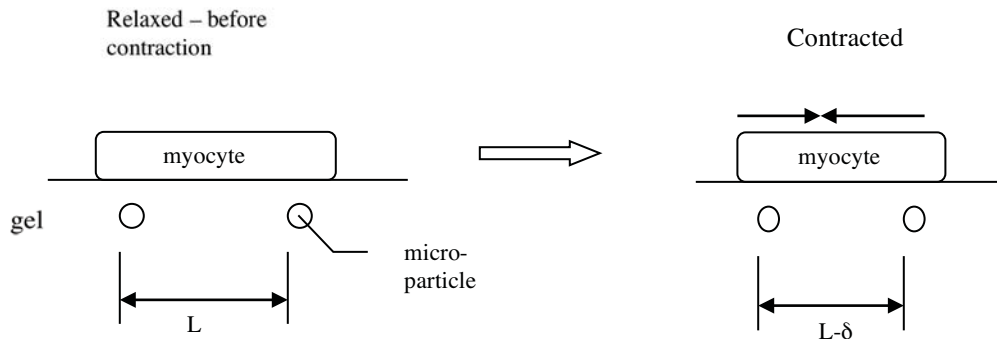
A cell migrates along a rigid substrate due, for example, to a chemotactic gradient. In an attempt to provide a somewhat more realistic environment for the cell, the medium viscosity, μ_m is increased many-fold above the normal value for culture medium (which has a viscosity similar to that of water). The cell is observed to travel at speed V , and can be modeled as a disk-shaped object of diameter, D , height, h ($\ll D$), and has an internal viscosity μ_c .

- a) Obtain a *scaling relation* (an order of magnitude estimate) for the drag force experienced by the cell due to the viscous culture medium, expressed in terms of the quantities given above.
- b) At what value of μ_m would you expect that this external shear stress would have a significant effect on the migration speed of the cell? Provide a brief (one or two sentence) explanation of your reasoning.
- c) Now consider the case in which the medium flows past the cell in a direction opposite to the direction of cell migration, so that the velocity gradient (shear rate) at the cell surface is dv/dz , where z is measured perpendicular to the surface of the cell. d) Estimate how large dv/dz would need to be in order to cause the cell to stop, i.e., $V = 0$? You may assume that the average adhesion force per unit area is f_a .

3 -- Myocyte contraction

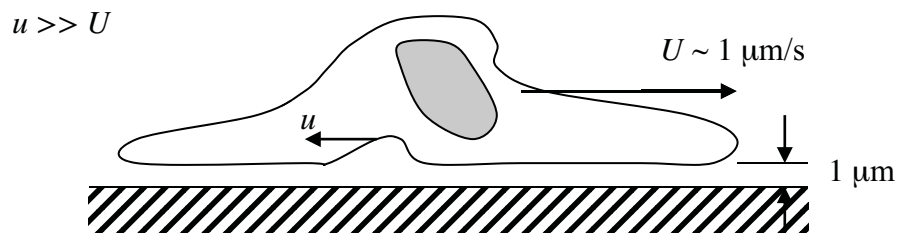
A new experimental technique determines the strength of contraction of a cardiac myocyte (the contractile cells in the heart) by measuring the force it exerts on the substrate on which it is grown. To measure this force cells are grown on an incompressible gel that has a sufficiently low elastic modulus such that it deforms by a measurable amount in response to the forces generated by the cells and transmitted to the gel. In order to monitor these deformations, fluorescent microparticles are embedded in the gel and the change in separation distance between particles as a result of the contraction is measured. You may model the cell as a disk-shaped object with diameter D and assume that it remains firmly attached to the gel. (Note that myocytes are normally elongated, but are modeled here as disk-shaped for simplicity.)

- a) Given that the two particles in the sketch immediately beneath the cell are separated by a distance L ($\sim D$) prior to cell contraction, and $L - \delta$ just afterward, and that the Young's modulus of the gel is E_g , obtain an estimate for the contractile force generated by the cell, F .
- b) Describe what you would expect to find if you monitored two microparticles located in the gel as shown in the sketch below, but positioned *perpendicular* to the direction of cell contraction, but in a plane parallel to the gel surface. Would they move closer together or further apart? Roughly by how much relative to δ ?



4 – Gliding bacterium

Gliding bacteria move by generating a shear flow between themselves and a substrate. The flow is thought to be generated by forcing their membrane to undergo rhythmic peristaltic contractions as shown in the sketch below. As a simple estimate of the efficiency of this type of motion, calculate the energy required to propel a gliding bacterium $0.1 \mu\text{m}$ above a surface. You may assume that the liquid medium is water (viscosity $10^{-3} \text{ Pa}\cdot\text{s}$) and that the typical area of the sheared zone is $100 \mu\text{m}^2$.



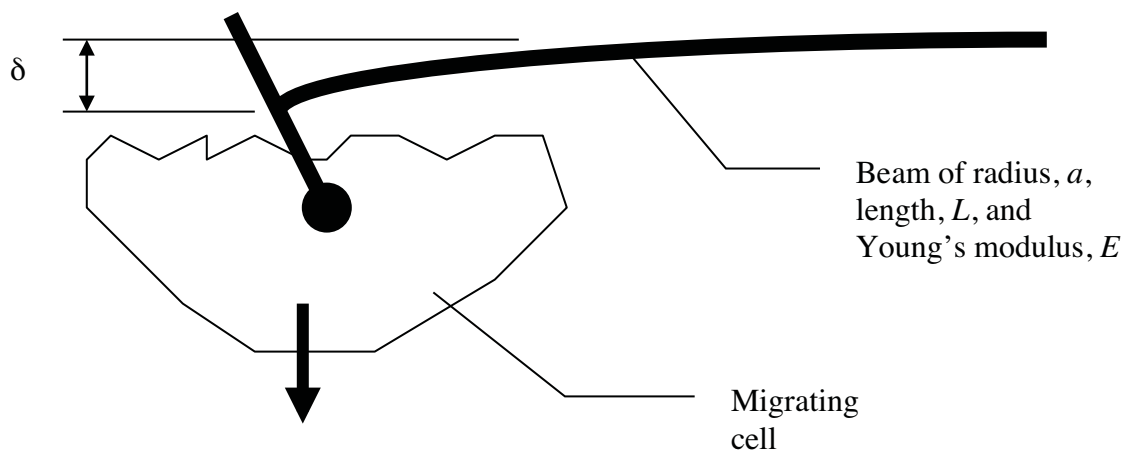
5 -- Cantilever Beam Cell Probe

A method used to measure the forces that can be generated by a migrating cell is shown in the sketch. One tip of a T-shaped probe is coated with adhesion molecules and attached to the upper surface of a migrating cell. As the cell migrates along the surface, it pulls the probe, producing a detectable deflection, δ . The probe is rigidly attached at its base. The main section of the probe is circular in cross-section with radius a and length L , and is made from a material with Young's modulus E .

- Obtain an expression for the force generated by the cell in terms of the deflection (δ), and the dimensions and properties of the probe.

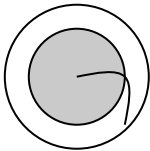
b) Now consider the migrating behavior of the cell. Discuss how would you expect the maximum force generated by the cell to change in each of the following situations:

1. The concentration of adhesion sites on the substrate on which the cell is migrating is increased (for a disk-shaped cell).
2. An agent (e.g., colchicine) is introduced that causes disruption of the microtubules.
3. The contact area between the cell and the probe tip is increased.



6 – Bacterial motility

Recall from the discussion in the chapter on flagella and cilia, that bacteria typically drive their motion by a fundamentally different mechanism in which the flagellum, which is generally helical in shape, is driven in a rotary fashion by a molecular motor at its base. Consider a flagellum having the geometry shown in the sketch in which a helix of radius a is rotated at constant speed ω . If the total length of the flagellum, measured along the axis, is L , and the viscous drag per unit length along the filament is $K_n \omega_n$ for flow normal to the filament and $K_t \omega_t$ for flow tangential to it, where ω_n and ω_t are the normal and tangential components of flagellar speed, obtain an expression for the total propulsion force provided by the flagellum.

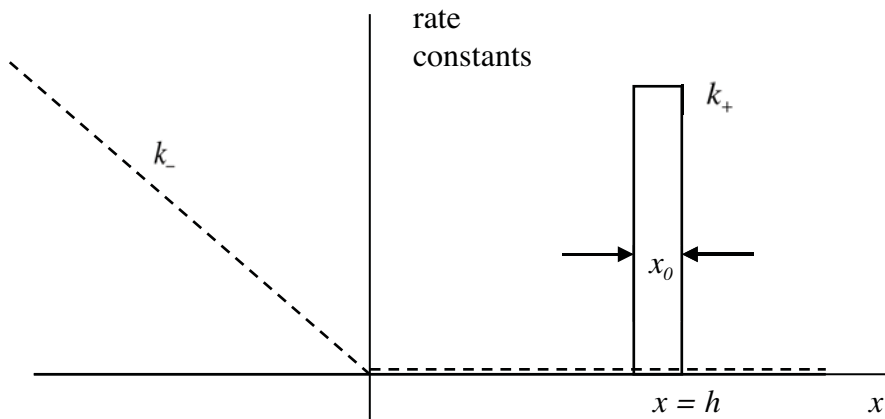


view looking from the back along
the axis of the flagellum

7 – Cross-bridge model

The cross-bridge model presented in class and in the notes presents the basic concepts, but is obviously idealized. Over the years, researchers have proposed various functional forms for the binding and unbinding rate constants (k_+ and k_- , respectively). Here we explore one of those alternative descriptions in which k_- rises linearly for $x < 0$ with a slope of $-\alpha$ (see figure).

a) Drawing upon all the same assumptions as in the model presented in class, changing only the x -dependence of the unbinding rate constant as shown, obtain new expressions for the binding probability, $n(x)$ in each of the domains, the normalized force generated, F/F_{max} , and the normalized power, $(Fv)/(F_{max}v_{max})$.



b) Plot $n(x)$ for several different values of sliding velocity. Explain the observed behavior in terms of the maximum values attained and the length of the asymptotic tail in the range of $x < 0$.

c) Identify parameter values that produce a normalized force-velocity curve as obtained in (a) that agrees with Hill's equation

$$\frac{v}{v_{\max}} = \frac{1 - (F/F_{\max})}{1 + C(F/F_{\max})}$$

[see eqn. (20) in Chapter 2.3] with $C = 5$. Plot both relationships on the same graph. (There's no need match the two extremely well, I just want you to see how the different parameter values affect the curves.)

d) Describe in qualitative terms, the effect on $n(x)$ of having a large value for k immediately as x falls below zero (you can consider this in the context of the model presented in class with constant k for $x < 0$). Explain how this would affect the power that can be generated by the muscle or the efficiency of power generation.

8 – Bleb formation

In a recent publication (Charras, et al., 2005), a model is proposed for bleb formation as a consequence of internal acto-myosin contractility, leading to an increase in fluid pressure within the cytoskeleton that subsequently is released by the flow of fluid toward the cell membrane through the porous cytoskeletal matrix. A bleb is formed when fluid pressure reaches a level that it can separate the membrane from its tethers to the cortical cytoskeleton. In the supplemental material associated with that paper, a scaling analysis is proposed to predict the separation of the membrane from the cortical cytoskeleton, leading to the prediction that the critical bleb size is:

$$d_c \sim \left(\frac{T_0 J}{P^2}\right)^{1/2}$$

where J is the energy per unit area of adhesion, P is fluid pressure and T_0 is the membrane tension.

- a) Show how one can obtain the approximate form of the equation used in the analysis for the “free energy of detachment”.
- b) Explain in your own words how the size of the region of membrane separation is determined.
- c) Does this approach seem reasonable to you? Why or why not?

The relevant section of text from the Supplement is copied below:

“Starting with this picture for stress generation, the critical area of membrane detachment from the cytoskeleton needed for a bleb to start growing can be estimated. The free energy for the detachment of a small area of membrane of diameter d from the cortex, is $U \approx Pd^2\delta - Jd^2 - T\delta^2$ where P is the given hydrostatic pressure, δ the membrane deflection, J the membrane-cytoskeleton adhesion energy, and T the membrane tension. For small deflections, the membrane unwrinkles as it detaches, and can flow in the plane to accommodate blebbing. Therefore, the membrane tension is relatively uniform as the bleb starts forming, hence $T \approx T_0 \approx \text{constant}$. In this limit, solving $\frac{\partial U}{\partial d} = \frac{\partial U}{\partial \delta} = 0$ yields the critical bleb size $d_c \sim \left(\frac{T_0 J}{P^2}\right)^{1/2}$ above which a bleb will grow catastrophically in a pressure controlled situation; however, the limited volume of fluid available prevents this. Equating this critical size to the average distance between cytoskeletal-membrane anchors yields the minimum pressure for bleb growth. With $J \sim 10^{-4} \text{ J.m}^{-2}$ ¹⁰, $T_0 \sim 10^{-2} \text{ mN.m}^{-1}$ ¹¹, and $P \sim 300 \text{ Pa}$ (Figure S1), we get a nucleation size $d_c \sim 100 \text{ nm}$.

Finally, during retraction, myosin heads moving along actin filaments bring the bleb back towards the cell body forcing the cytosol back in. Assuming a constant pressure within the bleb because it only consists of cytosol, Darcy’s law implies that the cortex must exert a pressure $\Delta P \approx \frac{vd}{k}$ with v the retraction speed, d the stress diffusion length, and k the hydraulic permeability of the cytoskeleton. Applying the Laplace law, the cortical tension T_c due to actinomyosin contraction is $T_c \sim \Delta P R_b \sim \frac{vdR_b}{k}$. Assuming a homogeneous distribution of myosin motors in the hemispherical cortical shell, this implies that the force generated by the motors scales as $F \sim T_c R_b$. Therefore, the number of working motors is roughly $N \sim \frac{vdR_b^2}{kf_{myo}\omega_{myo}}$ where $f_{myo} \sim 1.5 \text{ pN}$ ^{12,13} is the force per myosin motor per cycle, $\omega_{myo} \sim 25 \text{ Hz}$ ¹⁴ is the myosin motor cycle frequency. With $d \sim 8 \text{ }\mu\text{m}$, $v \sim 0.1 \text{ }\mu\text{m.s}^{-1}$ (Figure 1D and S2), $k \sim 3.4 \cdot 10^{-15} \text{ m}^4 \cdot \text{N}^{-1} \cdot \text{s}^{-1}$ and $R_b \sim 5 \text{ }\mu\text{m}$, we get $N \sim 350$ myosin heads. This is a realistic number in view of the estimated number of myosins within a cell $N_{\text{total}} > 10^4$ ¹⁵.”

9 -- Nematode motility

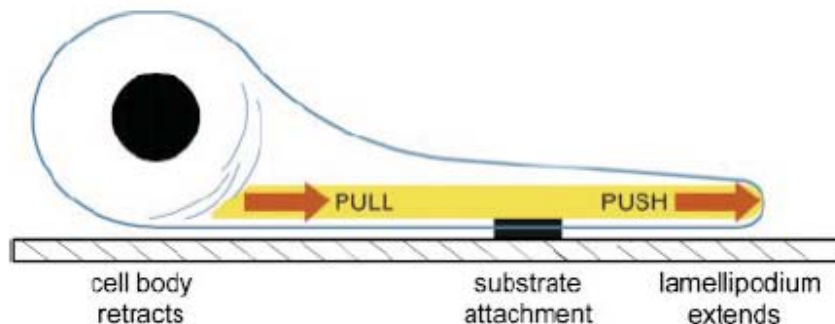
Nematodes have been observed to migrate by pseudopod protrusion and cell contraction, in a manner that appears quite similar to actin-based motility of other cell types. What distinguishes nematode migration, however, is that these cells lack actin, and use another filament-forming protein, major sperm protein (MSP). MSP differs from actin in several important respects:

- MSP filaments lack polarity, so cell contraction must not result from motor-induced contractility of motors that “walk” in a preferred direction along the filament.
- Unlike actin, MSP filaments form bundles without the aid of cross-linking proteins.
- Networks of MSP are thought to adhere to the intracellular face of the cell membrane in a pH-sensitive manner, so that a cell can modulate the strength of adhesion between the network and the membrane by adjusting local intracellular pH.

A recent paper describes nematode motility in the following way:

In summary, near the cell center, the crosslinking sites protonate, the hydrophobic bundling force weakens and the filament bundles begin to dissociate into their constituent filaments. Each filament that peels off a filament bundle can now shorten to its equilibrium length, L_0 ; this generates a nearly isotropic contractile stress. Because the substrate adhesive forces are less at the rear of the cell than at the front, this contractile stress pulls the cell body forwards, rather than pulling the cell front rearwards. Thus, bundling of filaments at the cell front and their subsequent unbundling at the cell rear constitutes a ‘push-pull’ motor that drives the cell forwards. Said another way, bundling creates both the protrusive force at the leading edge and the storage of elastic energy in the lamellipodial gel that is later released to generate the retraction force required to pull up the cell rear. (Bottino, et al., J Cell Sci, 2002)

In addition to the forward-acting force resulting from filament bundling, the familiar Brownian ratchet generates force at the leading edge of the protrusion. Together with an asymmetry in adhesion, associated with variations in pH, the nematode produces all the essential elements of migration: protrusion, adhesion, contraction, and rear release.



a) MSP forms filaments that, like actin, consist of monomers arranged in a double helical pattern. The individual MSP monomers are much smaller than actin, however, having a molecular weight of only 14kDa. Due to their smaller molecular weight, the filaments will be smaller in diameter. Given that the molecular weight of actin is 43 kDa, and its diameter is 4 nm, what would you estimate to be the diameter of an MSP monomer?

Assuming that the effective Young's modulus of an MSP filament is the same as that of an actin filament ($E \sim 2 \times 10^9$ Pa) and an actin filament has a persistence length of about $15 \mu\text{m}$, what will be the persistence length of a single MSDP filament?

b) Now consider the mechanism of network contraction. Consistent with the quote provided above, filaments near the cell center become protonated due to the locally lower pH, and this causes the filament bundles to start to unravel, with individual filaments becoming separated from the bundles. When bundled, the proteins tend to assume a length in the fiber approximately equal to their contour length, and enthalpic effects dominate fiber elasticity. As individual filaments separate from the bundle due to protonation, they tend to want to shorten due to entropic effects that cause them to assume a more random configuration. Consider just a single bundle, consisting of a collection of N filaments and assume that as they bundle, they become close-packed and adhere tightly to each other with no relative slippage when the bundle bends. Because they are bundled, each filament within the bundle is initially at a length nearly (*but not quite!*) equal to its contour length, L . As the individual filaments separate, one-by-one, a new equilibrium is reached in which those filaments that have separated from the bundle are in tension, stretched beyond their rest length, and those filaments remaining in the bundle are in compression.

First, obtain an expression for the difference between the rest length of a single filament and its contour length, assuming that the filament, because of its large persistence length, *remains nearly straight*.

Now consider all filaments in a bundle to be in parallel and tethered to fixed points at the two ends, and that there is no net force exerted at the ends of each bundle. Obtain an expression for the difference between the rest length of the bundle and its contour length, given the assumptions stated above. (Hint: Note that the individual filaments are nearly straight, due to their long persistence length, *whether or not* they are bundled.)

c) As a bundle starts to unravel, some of the filaments will be acting as though they are free while others will continue to act as part of a bundle. All filaments continue to be tethered at the same two endpoints. Explain the state of tension or compression in the two groups of filaments (free or bundled), and the net effect this has on the distance between the two endpoints, which you can assume are still under zero net force.

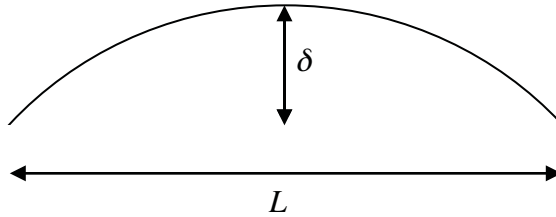
Explain how you would compute the new rest length of this collection of filaments, some of which are free and some of which remain part of the bundle.

d) Consider now, the forces exerted by the tips of the filaments on the cell membrane, and the response of the membrane in two limiting cases, when either tension or bending stiffness dominate. In both cases, you may assume that the filaments exert an average normal force f per filament, that the force is uniformly distributed over the entire surface of the membrane at the leading edge of the protrusion (and is everywhere normal to it), and the number of filaments per unit area of membrane is ρ_f [# filaments/m²].

Case (i) (*membrane tension dominates so that the bending stiffness can be ignored*) Calculate the tension in the membrane. You may assume the surface tension, N , is equal in all directions, and that the local radii of curvature of the membrane are R_1 and R_2 (in two mutually perpendicular planes), with $R_1 \ll R_2$.

Case (ii): (*membrane bending dominates so that tension can be ignored*). Calculate the bending stiffness of the membrane K_b , assuming that the bending occurs in just a single plane. The geometry of the membrane is characterized by the two characteristic lengths, L and δ , as defined in the sketch.

What condition must be satisfied for bending stiffness to dominate over tension?

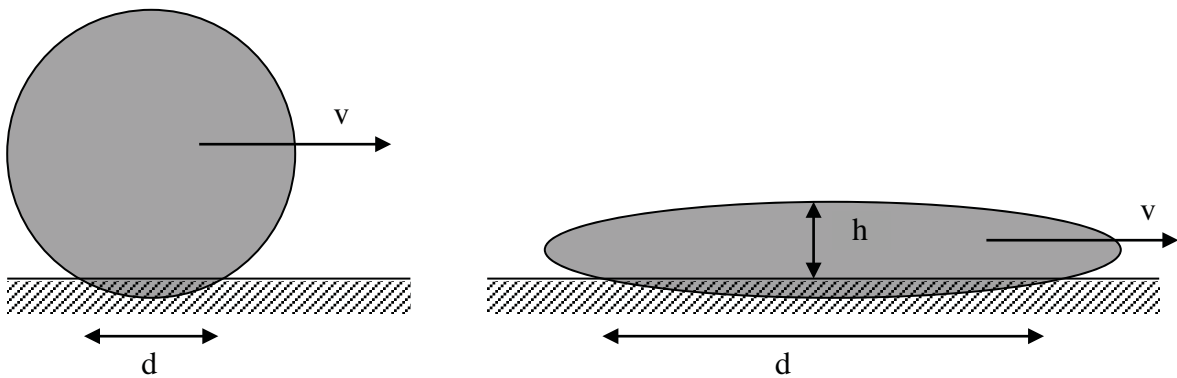


Cell migration model

Consider the following simple model for cell migration. A "cell" contains a Newtonian fluid of viscosity μ and adheres to the substrate beneath it with an adhesion force per unit area f_a . Depending on the strength of adhesion (e.g., the density of bonds or the adhesive force per bond) the cell takes on different configurations at the two limits of adhesive strength as shown in the figure. In the limit of small f_a , the cell rounds up so that the contact made with the substrate is confined to an area of diameter d which is small compared to the dimension of the entire cell. In the limit of large f_a , the cell flattens into a "pancake" shape with contact diameter d which is large compared to the height of the cell, h .

To analyze the cell's motion, we assume a balance between the power generated by the actin myosin motors that lead to an internal force F (that must be in balance with the external adhesive forces, $f_a d^2$) and the rate of viscous dissipation inside the cell. Note that the dissipation external to the cell can be neglected both due to the low velocities there and the low viscosity relative to the cell cytoplasm. As the cell migrates, the internal dissipation which is confined to a region that scales as d^3 in the rounded cell, but $d^2 h$ in the flattened cell.

- Obtain scaling relationships for the two limits described above that describes the dependence of the velocity of the migrating cell v as a function of the parameters, μ , f_a , d , and V where V is the cell volume. Compare your scaling predictions to the experimental data presented in class.
- How might this simple model be improved upon?



3.3.9 Bibliography

- Alberts, B., A. Johnson, et al. (2002). Molecular Biology of the Cell, Garland Pub.
- Chang, G., R. H. Spencer, et al. (1998). "Structure of the MscL homolog from *Mycobacterium tuberculosis*: a gated mechanosensitive ion channel." Science **282**(5397): 2220-6.
- Cukierman, E., R. Pankov, et al. (2001). "Taking cell-matrix adhesions to the third dimension." Science **294**(5547): 1708-12.
- Dembo, M. and Y. L. Wang (1999). "Stresses at the cell-to-substrate interface during locomotion of fibroblasts." Biophys J **76**(4): 2307-16.
- Dewey, C. F., Jr., S. R. Bussolari, et al. (1981). "The dynamic response of vascular endothelial cells to fluid shear stress." J Biomech Eng **103**(3): 177-85.
- Felder, S. and E. L. Elson (1990). "Mechanics of fibroblast locomotion: quantitative analysis of forces and motions at the leading lamellas of fibroblasts." J Cell Biol **111**(6 Pt 1): 2513-26.
- Gullingsrud, J., D. Kosztin, et al. (2001). "Structural determinants of MscL gating studied by molecular dynamics simulations." Biophys J **80**(5): 2074-81.
- Haidekker, M. A., N. L'Heureux, et al. (2000). "Fluid shear stress increases membrane fluidity in endothelial cells: a study with DCVJ fluorescence." Am J Physiol Heart Circ Physiol **278**(4): H1401-6.
- Harris, A. K., Jr. (1984). "Tissue culture cells on deformable substrata: biomechanical implications." J Biomech Eng **106**(1): 19-24.
- Howard, J. (2001). Mechanics of Motor Proteins and the Cytoskeleton, Sinauer Assoc.
- Huxley, A. F. (1957). "Muscle structure and theories of contraction." Prog Biophys biophys Chem **7**: 255-318.
- Huxley, A. F. and R. Niedergerke (1954). "Structural changes in muscle during contraction. Interference microscopy of living muscle fibers." Nature **173**: 971-973.
- Huxley, H. E. and J. Hanson (1954). "Changes in the cross-striations of muscle during contraction and stretch and their structural interpretation." Nature **173**: 973-973.
- Ives, C. L., S. G. Eskin, et al. (1986). "Mechanical effects on endothelial cell morphology: in vitro assessment." In Vitro Cell Dev Biol **22**(9): 500-7.
- Johnson, K. L., K. Kendall, et al. (1971). "Surface energy and the contact of elastic solids." Proceedings of the Royal Society **A324**: 301-320.
- Kolodney, M. S. and R. B. Wysolmerski (1992). "Isometric contraction by fibroblasts and endothelial cells in tissue culture: a quantitative study." J Cell Biol **117**(1): 73-82.
- Lauffenburger, D. A. and J. J. Linderman (1996). Receptors: Models for Binding, Trafficking, and Signaling. Oxford, Oxford University Press.
- Lehenkari, P. P. and M. A. Horton (1999). "Single integrin molecule adhesion forces in intact cells measured by atomic force microscopy." Biochem Biophys Res Commun **259**(3): 645-50.
- Lehninger, A. L., D. L. Nelson, et al. (2000). Lehninger Principles of Biochemistry. New York, Worth Publishers.
- Lighthill, J. (1969). "Hydromechanics of aquatic animal propulsion--a survey." Ann Rev Fluid Mech **1**: 413-446.
- Lodish, H., A. Berk, et al. (2000). Molecular Cell Biology. New York, W H Freeman & Co.
- McMahon, T. (1984). Muscles, Reflexes, and Locomotion. Princeton, Princeton University Press.

- Oberhauser, A. F., P. E. Marszalek, et al. (1998). "The molecular elasticity of the extracellular matrix protein tenascin." *Nature* **393**(6681): 181-5.
- Palecek, S. P., J. C. Loftus, et al. (1997). "Integrin-ligand binding properties govern cell migration speed through cell-substratum adhesiveness." *Nature* **385**(6616): 537-40.
- Pate, E., H. White, et al. (1993). "Determination of the myosin step size from mechanical and kinetic data." *Proc Natl Acad Sci U S A* **90**(6): 2451-5.
- Peskin, C. S., G. M. Odell, et al. (1993). "Cellular motions and thermal fluctuations: the Brownian ratchet." *Biophys J* **65**(1): 316-24.
- Sawada, Y. and M. P. Sheetz (2002). "Force transduction by Triton cytoskeletons." *J Cell Biol* **156**(4): 609-15.
- Sumpio, B. E., A. J. Banes, et al. (1988). "Alterations in aortic endothelial cell morphology and cytoskeletal protein synthesis during cyclic tensional deformation." *J Vasc Surg* **7**(1): 130-8.
- Svitkina, T. M., A. B. Verkhovsky, et al. (1997). "Analysis of the actin-myosin II system in fish epidermal keratocytes: mechanism of cell body translocation." *J Cell Biol* **139**(2): 397-415.
- Tskhovrebova, L., J. Trinick, et al. (1997). "Elasticity and unfolding of single molecules of the giant muscle protein titin." *Nature* **387**(6630): 308-12.

MIT OpenCourseWare
<http://ocw.mit.edu>

20.310J / 3.053J / 6.024J / 2.797J Molecular, Cellular, and Tissue Biomechanics
Spring 2015

For information about citing these materials or our Terms of Use, visit: <http://ocw.mit.edu/terms>.